REVIEW

Open Access

Recent application of Raman spectroscopy in tumor diagnosis: from conventional methods to artificial intelligence fusion

Yafeng Qi[1], Yuhong Liu[1*] and Jianbin Luo[1]

*Correspondence:
liuyuhong@tsinghua.edu.cn

[1] State Key Laboratory
of Tribology in Advanced
Equipment, Tsinghua University,
Beijing 100084, China

Abstract

Raman spectroscopy, as a label-free optical technology, has widely applied in tumor diagnosis. Relying on the different Raman technologies, conventional diagnostic methods can be used for the diagnosis of benign, malignant and subtypes of tumors. In the past 3 years, in addition to traditional diagnostic methods, the application of artificial intelligence (AI) in various technologies based on Raman technologies has been developing at an incredible speed. Based on this, three technical methods from single spot acquisition (conventional Raman spectroscopy, surface-enhanced Raman spectroscopy) to Raman imaging are respectively introduced and analyzed the diagnosis process of these technical methods. Meanwhile, the emerging AI applications of tumor diagnosis within these methods are highlighted and presented. Finally, the challenges and limitations of existing diagnostic methods, and the prospects of AI-enabled diagnostic methods are presented.

Keywords: Raman spectroscopy, Raman imaging, SERS, Artificial intelligence, Tumor diagnosis

Introduction

Tumor is a serious threat to human life and health of major diseases. Malignant tumor (cancer) is one of the main causes of human death. According to an estimation from the world health organization (WHO) in 2019, cancer is the first or second leading cause of death before age 70 in 112 countries, ranking the third or fourth in the other 23 countries [1]. Because of the lack of cancer screening and cognitive deficiency for the strategy of "early detection, early diagnosis and early treatment", the high or low 5 years of tumor patient survival rate becomes one of the key elements of life quality index.

At present, there are three main methods to detect tumors: tumor markers, imaging, and histopathology. The tumor marker detection is used for early tumor monitoring from the perspective of molecular biology, which is susceptible to individual differences and certain benign diseases [2–4]. Only several kinds of cancers have specific markers, such as alpha-fetoprotein, a tumor marker of liver cancer. Imaging diagnosis method is usually only used as an auxiliary means in clinical practice [5–7]. Because imaging diagnosis method only can initially identify of the shape and size of the tumor, can't

accurately identify the benign and malignant tumors qualitatively, with the high false positive ratio. Histopathology is the "gold standard" for the clinical application of tumor diagnosis [8–10], which can be traced back 100 years [11]. In this method, the benign and malignant, cell type and cancer subtype as well as the stage of the tumor can be identified by means of biopsy from the tissue and cell scale for further treatment of tumor. However, histopathology is a very complex subject with high professional and experience requiring for a long training cycle. To sum up, the existing methods of clinical cancer diagnosis have the problems of long diagnosis time, severe trauma, and high misjudgment rate, and relying heavily on the subjective experience of doctors.

Tissue and cell carcinogenesis are a very complex process, which will affect the content and structure of nucleic acids, proteins, and other biological macromolecules [12]. Therefore, there are differences in the morphology and composition of normal tissue/cell and cancerous tissue/cell at the molecular and/or cellular levels. Meanwhile, these differences can be detected optically, in the form of different intensity, peak location, peak width, etc. [13]. Then the position and/or intensity of these peaks can be analyzed corresponding to the transformation of cells and tissues, so as to realize the monitoring and diagnosis of tissue and cell cancerization [14].

Raman spectroscopy is a light scattering technique, whereby utilizes the differences between incident light wavelength ($\lambda_{incident}$) and scattering light wavelength ($\lambda_{scattering}$) for chemical analysis [15]. The elastic scattering is called Rayleigh scattering ($\lambda_{scattering} = \lambda_{incident}$), where the inelastic scattering is called Raman scattering which divided into anti-Stokes Raman scattering ($\lambda_{scattering} < \lambda_{incident}$) and Stokes Raman scattering ($\lambda_{scattering} > \lambda_{incident}$). Meanwhile, Raman spectroscopy, a label-free optical technology with the advantages of specificity, can also be used to analyze the biochemical characteristics of substances by such factors as the position and/or intensity of Raman peak [16]. Since the content and structure of biomacromolecules will change in the process of tissue and cell carcinogenesis, while Raman spectroscopy is mainly based on the interaction between light and molecules to obtain the information of molecular vibration and rotation. Therefore, we utilize the Raman spectroscopy to tumor detection. Spontaneous Raman scattering, as a rare phenomenon in comparison with its counterpart Rayleigh scattering, is typically identified as an insensitive technique [15]. However, with the technological advancement of highly efficient laser sources, low-noise detectors, valid filters and high-throughput optics, this applicability has significantly improved [17–19]. The commercial instrument "Confocal Raman Microscope", which integrates the optical magnification power of laser and direct visualization of the sample, has widely applicated in tumor diagnosis.

Although the confocal Raman microscope can integrate the optical magnification power of laser and direct visualization of the sample and has widely applicated in tumor diagnosis, the intensity of spontaneous Raman scattering signal is weak and the anti-interference ability is poor. In practical applications, it usually takes a long integration time to obtain the spectrum with acceptable signal noise ratio (SNR), which is not conducive to spectral acquisition and fast image formation. Given these shortcomings, surface-enhanced Raman spectroscopy (SERS), a very excellent Raman enhancement technology, is based on the combination of Raman spectroscopy and nanomaterials, which can realize highly precise target detection [20–22]. The SERS phenomenon

occurs on the local surface of some specially prepared metal or nonmetal conductor, where mainly caused by two mechanisms, called chemical enhancement mechanism and electromagnetic enhancement mechanism [20]. The former mainly emphasizes the adsorption between the metal substrate and adsorbed molecules, while the latter mainly for local field and dipole emission [23]. Thus, when adsorbed to a biomolecule, these nanoparticles result in greatly enhanced Raman spectrum signal by plasmon resonance. Recently, with high specificity, high sensitivity, rapidity and trace analysis, SERS is getting more and more frequently investigated in the field of tumor diagnosis.

Raman imaging technique is to study the molecular structure and dynamic characteristics by the interaction between light and matter [24, 25]. It can not only obtain the spectral information of light emission, absorption, and scattering, as well as the three-dimensional spatial imaging information, but also obtain the geometric shape, molecular structure, and dynamic characteristics of the research object [26, 27]. Hence, Raman imaging can be applied to the rapid imaging of tumor tissues to diagnose the subtypes and types of tumors according to the morphological and color changes of the imaging results [14, 28–30]. Especially the stimulated Raman histology (SRH), a label-free optical imaging method, provides rapid, label-free, sub-micrometer-resolution images of unprocessed biologic tissues, which has achieved rapid tumor diagnosis combining deep learning [31].

Based on widely applications of the Raman spectroscopy in the cancer diagnosis field, this article reviews the latest research and progress in the application of Raman spectroscopy in tumor diagnosis published between 2020 and 2022. It is mainly introduced from three aspects: Raman spectroscopy for tumor diagnosis, SERS for tumor diagnosis, Raman imaging for tumor diagnosis (Fig. 1). The conventional Raman spectra usually are utilized for tumor diagnosis by single spot acquisition, with simplicity but weak-signal highlighted. Therefore, the SERS are combined the Raman scatting and nanomaterials to enhance the Raman signal for tumor diagnosis, with high specificity, high sensitivity. However, these two techniques only leverage the Raman signal collected from the samples, but ignoring the morphological or positional information, especially in cells or tissues, which will affect the accuracy of diagnosis. Raman imaging technology can not only utilize the collected Raman signal, but also display the morphology or location
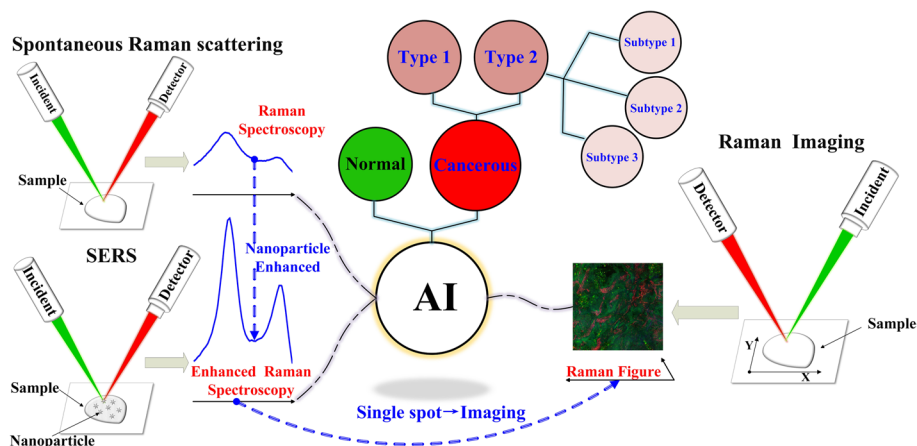

Fig. 1 Schematic illustration of AI application of Raman spectroscopy and Raman figures for cancer diagnosis

information of the samples, which greatly improves the carrying capacity of the output information, but also increases the complexity of information processing. Whereas facing these complex Raman images, artificial intelligence (AI) has shown greater processing power for tumor diagnosis. Herein, the conventional procedure for tumor diagnosis based on three aspects are overviewed, with the introduction of the AI application in this data processing procedure. Through the introduction of the above three aspects, Raman spectroscopy will be a novel scientific approach for tumor diagnosis in the future. Especially, Raman imaging analysis combined with artificial intelligence may even replace the diagnosis process of pathologists, which will greatly promote the medical development of intelligent tumor diagnosis.

Raman spectroscopy for tumor diagnosis

Raman spectroscopy can be easily collected from the commercial instrument "Confocal Raman Microscope", which has widely applied in tumor diagnosis. Data processing is vital for tumor diagnosis based on Raman spectroscopy. Conventional spectrochemical analysis methods are to process the original Raman data through several simple algorithm and then output the results, manually identify the difference between the output data of normal samples and cancerous samples, and judge the belonging of unknown samples, such as such as principal components analysis (PCA), linear discriminate analysis (LDA), quadratic discriminant analysis (QDA), partial least squares (PLS), etc. [32]. These methods have great advantages in the processing of small sample data. However, with the development of technology, the amount of data obtained has increased significantly, making it difficult to calculate and extract subtle variations in complex hidden features from big data by conventional methods. Machine learning is a system that can acquire and integrate knowledge autonomously, find hidden features to significantly amplify the difference between normal and cancerous samples, and independently judge the affiliation of unknown samples, such as support-vector machines (SVM), random forest (RF), etc. Machine learning has been widely used in the field of biomedical photonics. In addition, AI is a kind of computational model abstracting the neural network of human brain from the perspective of information processing. It has the characteristics of nonlinear, unlimited, strong adaptability and fault tolerance. In contrast, non-AI methods mainly start from the data itself, extract features through matrix transformation and other methods, and finally conduct classification and regression through modeling. In this chapter, we first introduce the conventional procedure in tumor diagnosis based on Raman spectroscopy, and then focus on the AI application in tumor diagnosis.

Conventional procedure

The conventional procedure for tumor diagnosis based on Raman spectroscopy necessitates (i) sample preparation; (ii) spectral acquisition; (iii) data processing and analysis. Raman microscope mainly collect the Raman spectroscopy from the tissues, cells, body fluids, and other raw materials. After collecting spectra, Raman spectroscopy data are used multiple methods for computational processing and analysis. Conventional methods for diagnosing Raman spectroscopy data usually utilize Raman peak intensity comparison or various multivariate statistical analytical methods. Cancers in different parts of the body have been diagnosed among these

conventional methods, such as: brain cancer [33–40], breast cancer [41–44], esophagus cancer [45], leukemia [46], liver cancer [47], lung cancer [48–50], oral cancer [51, 52], ovarian cancer [53], salivary gland neoplastic [54], rectal cancer [55], skin cancer [56, 57] (Table 1).

For sample preparation, tissues are the most directly and widely collected for tumor diagnosis. About the tissues, most researcher prefer to utilize the unprocessed surgical tissues, because the processed procedures of formalin fixation paraffin-embedding (FFPE) may influence Raman spectroscopy measurements. Indeed, Ning et al. [41] evaluated the diagnosis analysis capabilities of unprocessed surgical samples and dewaxed FFPE samples by collecting the Raman spectroscopy from different tissues (Fig. 2a). The results demonstrated that the dewaxing process significantly altered the biochemical composition of the tissues, particularly lipids, proteins, and carotenoids. Even though, the analytical result showed that PCA-LDA method and PLS-discriminate analysis (DA) method could distinguish the target tissue types effectively with satisfying overall accuracy in which the former of 88.3%, the matter of 93.0%. Although this study confirmed that FFPE sections had diagnostic potential with multivariate analytical model, biochemical changes still emerged, which may influence the accuracy. Therefore, it is preferable to use untreated samples.

In addition to tissues, body fluids are also easily accessible samples that are widely used to monitor various bodily functions and health conditions. Raman spectroscopy, a label-free analytical technique, has been proven useful in probing the blood components and the whole blood for over 40 years [93]. Blood is a vital bodily fluid responsible for numerous physiological functions, which contains plasma, erythrocytes (red blood cells), leucocytes (white blood cells) and platelets (thrombocytes). When an organ of the body becomes cancerous, the biochemical changes to the composition of blood follows. Therefore, researchers have utilized Raman spectroscopy to detect the changes for tumor diagnosis. For example, brain cancer [40], esophageal cancer [45], lung cancer [49]. In addition to blood as an important body fluid, saliva and urine are also readily available body fluids for tumor diagnosis. Raman spectra combined with saliva and/or urine have applied for tumor diagnosis, such as oral squamous cell carcinoma [52]. Particularly, Maitra et al. [45] collected Raman spectra from four kinds of human body liquid (plasma, serum, urine, saliva) to detect esophageal stages through to esophageal adenocarcinoma (Fig. 2b). For saliva and urine samples the analysis model achieved 100% classification for all classes, while for plasma and serum, the model achieved excellent accuracy in all esophageal stages (>90%).

Cells are more delicate at the detection scale than tissues, so cell detection based on Raman spectroscopy can be used for cancer screening. Raman spectroscopy on live cells can classify among different disease stages, and play a significant role clinically as a diagnostic tool for cell phenotype. For instance, breast cancer cells [44, 58], colorectal cancer cells [58, 59], lymphoma cells [60]. Besides, extracellular vesicles (EVs) secreted by cancer cells provide a crucial insight into cancer biology and could be leveraged to enhance diagnostics and disease monitoring. Penders et al. [92] present a single particle automated Raman trapping analysis (SPARTA) system, a dedicated standalone device optimized for single particle analysis of EVs (Fig. 2c). They

Table 1 Raman spectroscopy for tumor diagnosis

Sample	Methods	Diagnosis	Ref
Tissue	PLS-DA	Brain cancer	[33]
	PCA-LDA		[36]
	PCA		[37, 38]
	PCA-QDA		[39]
	PLS-DA	Breast cancer	[35]
	PCA-LDA, PLS-DA		[41]
	PCA-LDA		[42, 43]
	PCA-LDA	Liver cancer	[47]
	KCA, PCA	Lung cancer	[48]
	PLS-DA		[49]
	PCA-LDA		[50]
	PCA-LDA, PLS-LDA	Oral cancer	[51]
	PCA-LDA	Rectal cancer	[55]
	PLS-DA	Skin cancer	[56]
	PLS-DA		[57]
	Peak comparison	Ovarian cancer	[53]
Cell	PCA	Breast cancer	[44]
	PCA-LDA	Breast cancer	[58]
	PCA-LDA	Colorectal cancer	[58]
	PCA	Colorectal cancer	[59]
	PCA-QDA	Lymphoma	[60]
Serum	PCA-LDA	Brain cancer	[40]
	GA-QDA	Esophageal cancer	[45]
	PLS-DA	Lung cancer	[49]
Saliva	GA-QDA	Esophageal cancer	[45]
	PCA-LDA	Oral cancer	[52]
Plasma	GA-QDA	Esophageal cancer	[45]
Urine	GA-QDA	Esophageal cancer	[45]
Bone marrow superna-tants	PLS-DA	Leukemia	[46]
Tissue	SVM	Brain cancer	[61]
	RF, BT		[62]
	SVM	Breast cancer	[63]
	KNN	Cervical cancer	[64]
	SVM, KNN, RF, etc	Kidney cancer	[65]
	SVM		[66]
	SVM	Meningiomas	[67]
	1D-CNN	Bone tumors	[68, 69]
	1D-CNN	Breast cancer	[70]
	1D/2D-CNN	Chondrogenic Tumor	[71]
	1D-CNN	Colon cancer	[72]
	1D-CNN	Laryngeal cancer	[73]
	2D-CNN	Lung cancer	[74, 75]
	1D/2D-CNN		[76]
	1D-CNN	Oral cancer	[77, 78]
	1D/2D-CNN	Pancreatic cancer	[79]
	1D-CNN	Skin cancer	[80]

Table 1 (continued)

Sample	Methods	Diagnosis	Ref
Cell	SVM, RF	Bladder cancer	[81]
	SVM	Breast cancer	[82]
	RF	Breast cancer	[83]
	SVM	Central nervous system tumor	[84]
	SVM	Osteosarcoma	[69]
	KNN, SVM	Pancreatic cancer	[85]
Serum	RF, SVM	Brain cancer	[86]
	BT	Colorectal cancer	[87]
	SVM	Ovarian cancer	[88]
	SVM, KNN	Pancreatic cancer	[89]
	CNN	Brain cancer	[90]
	RNN, CNN	Brain cancer	[91]
	RNN, CNN	Lung cancer	[91]
Plasma	SVM	Ovarian cancer	[88]
Urine	SVM	Ovarian cancer	[88]

BT Boosted tree, *CNN* Convolutional neural network, *GA* Genetic algorithm, *KCA* K-means cluster analysis, *KNN* K-nearest neighbors, *LDA* Linear discriminate analysis, *PCA* Principal component analysis, *PLS-DA* Partial least squares discriminant analysis, *QDA* Quadratic discriminant analysis, *RF* Random forest, *RNN* Recursive neural network, *SVM* Support-vector machines
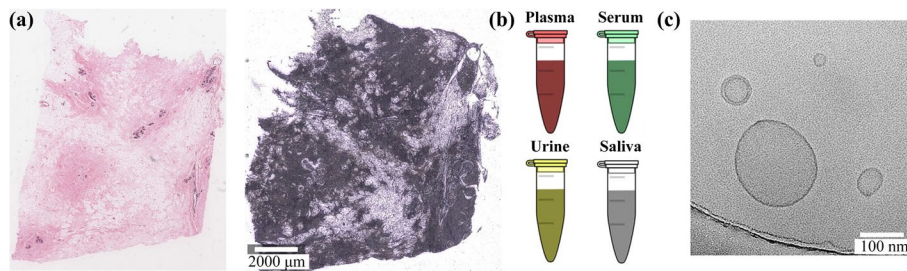

Fig. 2 Sample preparation for tumor diagnosis by Raman spectroscopy **a** White light micrographs of stained and unstained frozen healthy breast tissue section [41]; **b** Raman spectra of human body liquid (plasma, serum, urine, saliva) to identify cancer [45]; **c** Cryo-transmission electron microscope image of EVs [92]

demonstrate that the dedicated SPARTA system can differentiate between cancer and noncancer EVs with a high degree of sensitivity and specificity (> 95% for both).

After sample preparation, it turns to collect Raman spectroscopy from sample. The commercial instrument "Confocal Raman Microscope", which integrates the optical magnification power of laser and direct visualization of the sample, has widely applicated for Raman spectroscopy data acquisition. Different instruments equip different wavelength lasers, where different wavelengths of excitation light produce different sampling effects. The scattering intensity of visible light is higher than near infrared (NIR), while the NIR excitation was used to minimize tissue autofluorescence. Therefore, the appropriate laser wavelength should be selected according to the samples.

Data processing is vital for classification of different types of tumor tissues. The acquired spectra are firstly filtered, normalized, and corrected then classified by a variety of algorithms and methods. The advantages, limitations and corresponding suitable application of different data processing methods are as Table 2. For the conventional

Table 2 Data processing, advantages, limitations and suitable application of classification methods

Methods	Data processing	Advantages	Limitations	Suitable application
Peak intensity analysis	• Peak intensity: I_{normal} vs I_{cancer} • Peak intensity ratio (R=I_{12xx}/I_{16xx}): R_{normal} vs R_{cancer}	• Straightforward • Simple	• Low accuracy • Data size increases, accuracy downs	• Obvious characteristic peaks and large differences • Small-scale sample data (10~100)
Multivariate statistical analysis	-	• High interpretability • Easily implement	• Facing lager amount data, accuracy has limitation	• Medium-scale sample data (100~1000)
PCA	• Reduces the original Raman spectra to PCs while preserving the features that contribute most to the difference in the Raman spectra	• Reduces data dimensionality to PCs • Retains important data information • Removes background noise	• Relatively low classification accuracy	• Unsupervised method • Exploratory study • Data-reduction algorithm
PLS	• Regression modeling for independent and dependent variables of Raman spectra	• Reduces data dimensionality to key factors • Better selects characteristic variables	• Relatively low classification accuracy	• Supervised method • Data-reduction algorithm
KCA	• Takes the mean of the nearest point to the seed constantly to cluster analysis of Raman spectra	• Simple algorithm principle • Fast processing speed	• K value is difficult to determine • Not necessarily global optimal, but only local optimal	• Unsupervised clustering technique • Exploratory study • Samples with large differences between groups
LDA	• Projects the Raman spectra into the vector space with the maximum between-class distance and the minimum within-class distance	• Commonest classification method • High accuracy	• Overfit if data insufficient	• Powerful supervised technique for classification • Integrates with PCA method
QDA	• Estimates the single covariance matrix for each type of Raman spectra	• Variant of LDA • High accuracy	• Can't for data dimension reduction	• Supervised technique for classification • Sample analysis
GA	• Feature extraction of Raman spectra, as a stage prior to classification	• Feature selection • Strong robustness	• Low computation speed • Complex programming process	• General optimization technique • Feature extraction of data
Classical machine learning	-	• Higher accuracy • Easily implement	• Poor in training efficiency when processing large-scale data	• Large-scale sample data (1000~10,000)
SVM	• Seeks to determine the optimal hyperplane that maximizes the distance between the hyperplane and the nearest Raman spectra data sample in a high-dimensional space	• Less prone to overfitting • Avoids local optimum and "curse of dimensionality"	• Poor training efficiency when processing large-scale data	• Nonlinear, multi-dimensional problems • Small sample learning problems
BT	• Changes the weight of Raman spectra data, learns multiple classifiers, and combines these classifiers linearly to improve the performance of classification	• Ensemble learning method • No need to do feature normalization	• Sensitive to abnormal data and • Easy to overfit	• Low dimensional data • Layers not too high

Table 2 (continued)

Methods	Data processing	Advantages	Limitations	Suitable application
RF	• Uses multiple trees to train and predict Raman spectra data	• Ensemble learning method • Low risk of overfitting	• Relatively lower learning speed	• Limited samples
KNN	• Uses proximity of a single Raman spectral data point to classify or predict groupings	• High precision • Insensitive to outliers	• Relatively large time complexity • Large space complexity	• Small-size samples • Low-dimensional data
Deep learning	-	• Higher accuracy • Good portability	• Large amounts of computation • Complex model design	• Larger-scale sample data (1000 +, 10,000 +, …)
CNN	• Raman spectra/figures as input data, prefers Raman figures as input • Extracts features from input data directly and classifies the observed objects	• Directly extracts features from input data • Classifies the observed objects • Simple architecture • Ease of use	• Depends on quality and features of the data	• Most of the modeling tasks (classification and regression)
RNN	• Raman spectra as input data • Mines wavenumber and intensity information in the Raman spectra data	• Strong learning ability of time series non-linear data behavior • Stores more long-term sequence information • Mines temporal and semantic information in the data	• Risks of gradient exploding and gradient vanishing	• Sequence data • Time series nonlinear data behavior • Classification and prediction

BT Boosted tree, *CNN* Convolutional neural network, *GA* Genetic algorithm, *KCA* k-means cluster analysis, *KNN* k-nearest neighbors, *LDA* Linear discriminate analysis, *PCA* Principal component analysis, *PLS* Partial least squares, *QDA* Quadratic discriminant analysis, *RF* Random forest, *RNN* Recursive neural network, *SVM* Support-vector machines

data processing methods, the Raman peak intensity comparison is the most straight-forward method [53], which usually utilizes the intensity of several characteristic peaks or the ratio of a pair of characteristic peaks to distinguish. This method is suitable for spectral data with obvious characteristic peaks and large differences, and is more effective for small sample data. Once the sample data size increases, the accuracy is not high. Therefore, for vast amounts of data, abundant multivariate statistical analysis methods are often used to analyze spectral differences and distinguish the tissues. The multivariate statistical analysis methods contain PCA [37, 38, 44, 48, 54] (Fig. 3a), PCA-LDA [36, 40–43, 47, 50–52, 55] (Fig. 3b), PLS-DA [33, 35, 41, 49, 56, 57] (Fig. 3c), PLS-LDA [51] (Fig. 3d), PCA-QDA [39, 60] (Fig. 3e), K-means cluster analysis (KCA) [48], genetic algorithm (GA)-QDA [45] (Fig. 3f). PCA can effectively reduce the spectrum to a certain number of principal components (PCs) that account for significant spectral variance, thus retaining important spectral data while removing background noise [94]. PLS is also a data-reduction algorithms, which can be used to reduce individual spectra down to a few key factors [95]. PCA is the unsupervised method and ideal for explora-tory studies but cannot distinguish well among samples that do not differ significantly between groups, while PLS is the supervised method where the characteristic variables of each group can be better selected to distinguish and the relationship between sam-ples can be determined. PLS can be shown to be better than PCA to prepare for clas-sification [96]. Although these two methods can also directly classify spectral data, the accuracy is relatively low, so classification methods need to be further used, which typi-cally rely on the clustering technique and discriminate analysis methods. KCA is a pop-ular option of the clustering technique, while LDA and QDA are the popular options of DA methods. For clustering technique, KCA method is an unsupervised clustering method of data exploration that helps to explore and discover data structures in a large amount of data with simple algorithm principle and fast processing speed [48]. How-ever, KCA method utilizes the K given in advance, where the choice of K value is dif-ficult to determine. And the result of KCA method is not necessarily global optimal, but

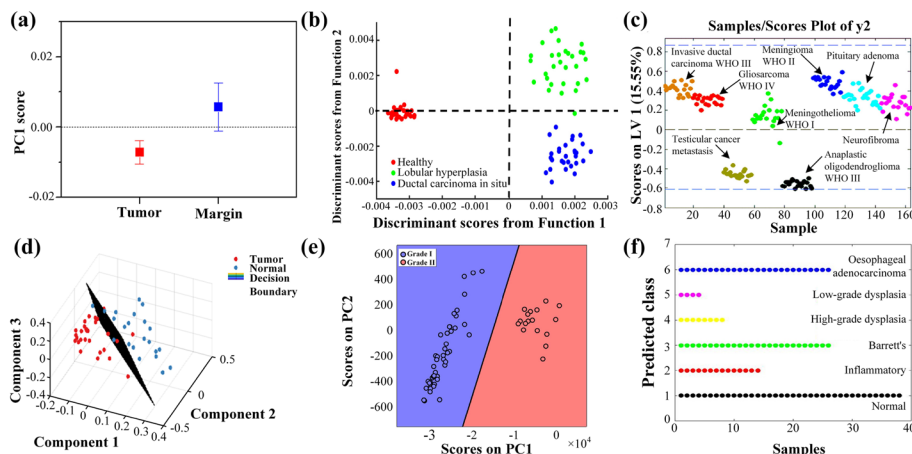**Fig. 3** Multivariate statistical analysis for tumor diagnosis by Raman spectroscopy **a** PCA analysis result of tumoral tissue and healthy margin [54]; **b** PCA-LDA analysis result of breast cancer [43]; **c** PLS-DA analysis result of different cancers [35]; **d** PLS-LDA analysis result of oral cancer [51]; **e** PCA-QDA analysis result of meningiomas [39]; **f** GA-QDA analysis result of esophageal cancer [45]

only local optimal. Therefore, KCA method is suitable for samples with large differences between groups. For DA methods, LDA is a powerful supervised technique for achieving class classification, but it can overfit if the number of spectra is insufficient [95]. Therefore, a general guideline for applying a supervised technique is to have the number of spectra 5–10 times bigger than the number of variables [97], for example, using a PCA prior stage, hence PCA-LDA. PCA-LDA is the commonest method among the multivariate statistical analysis methods. QDA is the variant of LDA, where the both have similar algorithm characteristics. The difference is that LDA should be used when the covariance matrix of different classified samples is the same, while the QDA should be used when the covariance matrix of different classification samples is different [98]. In addition, the downside of QDA is that it cannot be used as a dimension reduction technique. Genetic algorithm is a branch of evolutionary computing, which simulates natural selection and genetic mechanisms to find optimal solutions. Meanwhile, GA is a general optimization technique and is applied for feature selection, where the feature selection is commonly applied as a stage prior to classification as a means to prevent overfitting and to circumvent the "curse of dimensionality" [99]. Therefore, GA method can be used for feature extraction of data and then QDA classification method is used for sample analysis.

Although multivariate statistical analysis methods yielded high accuracy, these methods pose a limitation toward improving accuracy, especially facing large data sets. Therefore, it is critical to search more accurate methods for tumor diagnosis. With the development of computer science and technology, the machine-learning classification with neural network was applied for tissue diagnosis yielding higher sensitivity and specificity.

AI application

With the advances in artificial intelligence, machine learning (ML) has been applied in tumor diagnosis based on Raman spectroscopy with higher accuracy. Herein, the conventional ML methods, SVM, RF, have harvested high accuracy for many years. Recently, deep learning, a branch of the machine learning, has achieved more excellent accuracy for tumor diagnosis. From the literature, these ML methods have applied in different parts of the body, such as in bladder cancer [81], bone tumors [68], brain cancer [61, 62, 86, 90, 91], breast cancer [63, 70, 82, 83], central nervous system tumor [84], cervical cancer [64], chondrogenic tumor [71], colon cancer [72, 87], kidney cancer [65, 66], laryngeal cancer [73], lung cancer [74–76], meningiomas [67], oral cancer [77, 78], osteosarcoma [69], ovarian cancer [88], pancreatic cancer [79, 85, 89], skin cancer [80, 100, 101] (Table 1).

For classical ML methods, the advantages, limitations and corresponding suitable application of different ML methods are as Table 2. SVM is a generalized classifier for binary classification, which seeks to determine the optimal hyperplane that maximizes the distance between the hyperplane and the nearest data sample in a high-dimensional space [102]. SVM can avoid local optimum and "curse of dimensionality", and is less prone to overfitting. However, the prediction accuracy of SVM method highly depends on the kernel function, and SVM method has poor training

efficiency when processing large-scale data. Therefore, SVM method is powerful in dealing with nonlinear, multi-dimensional problems, peculiarly those with limited samples [103]. Nowadays, SVM is the most widely used method for tumor diagnosis based on Raman spectroscopy, whatever the tissues as original sample preparation [61, 63, 65–68, 77], or cells as original sample preparation [69, 81, 82, 85, 100, 101], body fluids as original sample preparation [84, 86, 88, 89]. Other ML methods, such as boosted tree (BT) [62, 87], k-nearest neighbors (KNN) [64, 65, 68, 85], RF [62, 65, 83], also have applied for tumor diagnosis. BT method is an ensemble learning method, whose main idea is to assemble a weak classifier into a strong classifier. When using the boosted tree approach as learning algorithm, there is no need to do feature normalization/normalization for different types of data, and it is easy to balance runtime efficiency and accuracy. Whereas, BT method is sensitive to abnormal data and easy to overfit. Hence, BT method is suitable for low dimensional data, and the number of model layers should not be too high. RF method, as an ensemble learning method, can effectively reduce the risk of overfitting by leveraging the strategy of bagging and random feature selection to construct several decorrelated decision trees and output their average predictions [104, 105]. But the RF method has relatively lower learning speed, which is willing to dealing with those with limited samples. KNN is a nonparametric, supervised learning classifier that uses proximity of a single data point to classify or predict groupings [106]. KNN method can yield high precision and is insensitive to outliers, while with relatively large time complexity and space complexity. Therefore, KNN method is suitable for small-size samples and low-dimensional data. O'Dwyer et al. [81] utilized 11 classification method for different grade bladder cancer cells and normal cells, including SVM, RF, PLS, PCA-LDA, PCA-QDA, PCA-KNN, marginal relevance (MR)-LDA, MR-QDA, MR-KNN, MR-RF, MR-SVM method (Fig. 4a). And the results showed that cells can be distinguished by using a variety of approaches with accuracy, sensitivity, and specificity in excess of

Fig. 4 AI method for tumor diagnosis by Raman spectroscopy **a** Different grade bladder cancer cell classification accuracy of the 11 classifiers [81]; **b** Three classic CNNs (AlexNet, ResNet, and GoogLeNet) model structure for diagnosis of glioma [90]; **c** RNN model structure for diagnosis of lung cancer and glioma [91]; **d** The conversion from the Raman spectral signal into 2D Raman spectrograms [74]; **e** Raman encoding figures [76]

95%, especially the SVM methods with the best performances of 0.996 accuracy, 0.996 sensitivity and 0.996 specificity.

For deep learning methods, convolutional neural network (CNN), one of the most popular basic deep leaning architectures, has been widely used tumor diagnosis based on Raman spectroscopy, where the original sample preparation can be obtained from tissues [68, 70, 73–80] and body fluids [90, 91]. CNN simulates the structure and function of biological neural networks in computers, which mainly contains three basic operations, i.e., the convolution, activation, and pooling. Convolution extracts the feature maps from the inputs with a kernel matrix, while the activation is to map its inputs into another space nonlinearly and is usually operated after the convolution, then pooling is a subsampling strategy, including max-pooling and average-pooling [32]. Indeed, a general CNN model is basically composed by several convolution, activation, and pooling layers and sometimes ties several fully connected layers. AlexNet, ResNet, and GoogLeNet are three kinds of classic CNNs, where the differences lie in the structure of the network. The initial AlexNet was proposed by Sutskever et al. [107] with 8 layers. It utilizes local response normalization to solve the overfitting problem and utilizes multiple GPUs to accelerate the performance of the model, shorten the training time, and balance the training speed and accuracy of the model [107]. The initial ResNet was proposed by He et al. [108] with 152 layers. It utilizes a residual algorithm to significantly improve the ability of a neural network to extract features. The use of residual blocks is to solve the vanishing and disappearing gradient problems with ordinary CNNs by not only deepening the depth of the network but also by improving the performance of the network [108]. The initial GoogLeNet was proposed by Szegedy et al. [109] with 22 layers. GoogLeNet introduces the "inception" new module, which connects filters with different sizes and dimensions into a new filter. Compared with other deep CNN models, GoogLeNet reduces the number of parameters and layers in the network and improves the utilization of computing resources inside the network [109]. After these excellent CNN models were proposed, researchers can further modify various models according to their own data, so as to establish required models and achieve high classification accuracy. In short, CNN can directly extract features from input data and classify the observed objects, but limited by the quality and features of the data. However, CNN is the first choice in most of the modeling tasks (classification and regression) because of the simple architecture and the ease of use. Tian et al. [90] utilized three classic CNNs, AlexNet, ResNet, and GoogLeNet, to build the classification model for diagnosis of glioma (Fig. 4b). The accuracy rates of the AlexNet, ResNet, and GoogLeNet models were 98.50%, 98.24%, and 99.50%, respectively, where GoogLeNet model yielded the best classification effect with the specificity and sensitivity of 98.98% and 98.48%, respectively. Meanwhile, other deep learning architectures are also used in tumor diagnosis and have achieved unprecedented success, such as recursive neural network (RNN) [91] (Fig. 4c). RNN is a type of neural networks with cyclic connections [110]. Compared with CNN, RNN has the characteristics of storing more long-term sequence information and mining temporal and semantic information in the data, which has a strong ability to learn the nonlinear data behavior of time sequence [91]. Considering the Raman spectroscopy can be regard as a special sequence, RNN may have more applications in Raman spectroscopy data classification.

Among these papers, most deep learning architectures utilized the Raman spectra as 1D data to fed into models for training and testing [68, 70, 77, 78, 80], however, 2D figures would be a better choice as inputs compared with 1D data for deep learning. Therefore, our group first proposed an unusual method wherein we considered the Raman spectral signal as a sequence and then converted it into a 2D Raman spectrogram by spectral short-time Fourier transform (SSTFT) [74, 75] (Fig. 4d). This novel method combined with deep learning yielded excellently accurate diagnosis of lung tissues. Subsequently, we extended the transformation approaches of converting the 1D Raman spectroscopy into 2D figures (Fig. 4e) and proposed a new concept called the Raman encoding figure, which can improve the accuracy [76]. Three new methods are proposed and implemented for the Raman spectrum conversion, i.e., spectral recurrence plot (SRP), spectral Gramian angular field (SGAF), and spectral Markov transition field (SMTF). For typical Raman spectrum, it contains two kinds of internal information, one for wavenumber position information, the other for intensity information. Particularly, SMTF is the conversion based on wavenumber position information, and SSTFT is the conversion based on wavenumber position information and intensity information. But for multiple spectra, they not only contain internal information, but also external information, such as shape information. Especially, SRP is the conversion based on structure of wavenumber series, while SGAF based on wavenumber series. The inclusion of different kinds of information in the conversion results in different performances. Furthermore, due to the more information involved in the transformation, SRP and SGAF methods are suitable for more complex original spectra, while SSTFT and SMTF are suitable for less varied spectra. These 2D-CNN methods all yielded more than 95% accuracy, 94% sensitivity, and 96% specificity when tested, where the SRP with best performances (98.9% accuracy, 99.5% sensitivity, 98.3% specificity), followed by SGAF, SSTFT, and SMTF. Meanwhile, we compared the diagnostic performances of the 2D-CNN method with that of the 1D-CNN method, which utilized the 1D Raman spectra as inputs and yielded a test accuracy of 94.1%, a test sensitivity of 91.8%, and a test specificity of 96.4%. In addition, Conforti et al. [71] proposed a chondrogenic tumor classification through wavelet transform of Raman spectra, which combines the hybrid 1D-2D deep learning classification process applied on Raman spectra both raw and after wavelet transform. The 1D deep learning classification makes it possible to distinguish between the tumor's early stages and more advanced ones with great accuracy, while the 2D deep learning classification yield the high accuracy classification between the tumor's malignant and non-cancerous stages, especially the 2D deep learning classification. Typical SSTFT method is limited by wavenumber (or frequency) resolution due to the application of a single wavenumber window. Here, Conforti et al.[71] proposed the continuous wavelet transform (CWT) method to solve this problem by using short windows at higher frequencies and long windows at lower frequencies, where the CWT method can be continuously changed during the procedure to still obtain a valid multi-resolution analysis. Finally, this method can classify Raman spectra obtained from bone tissues with high accuracy of 97% accuracy. This method extends the application of converting 1D Raman spectrum to 2D Raman encoding figure as deep learning input, and also shows that the conversion of 1D Raman spectrum to 2D Raman encoding figure has huge application space and can provide a reference method for tumor diagnosis based on Raman spectra. Overall, the 2D

Raman encoding figure combined with deep learning shows great potential for diagnosing tissues and may provide a novel analysis method for other spectral techniques.

In conclusion, the key of tumor diagnosis based on Raman spectroscopy is to find the difference between normal and cancerous samples. It is relatively unremarkable to look for such differences from the Raman characteristic peaks. Therefore, a variety of Raman spectral data methods have been developed to improve the diagnosis and recognition rate, from multivariate statistical methods, to classical machine learning methods, and finally to deep learning. Especially facing a large amount of data, deep learning can yield a better diagnosis and recognition rate. In the future, we should start from two aspects: data volume and further classification to achieve accurate diagnosis in view of the complexity of tumor diagnosis. On the one hand, the magnitude of sample data should be improved to explore the classification effect of various diagnostic methods in the case of large data volume and find better solutions. On the other hand, appropriate data processing methods should be selected for further typing of cancerous samples to achieve accurate diagnosis of cancerous subtypes.

SERS for tumor diagnosis

SERS is a very excellent Raman enhancement technology, which can realize highly precise target detection. SERS substrate preparation is the key of tumor diagnosis based on SERS, because the appropriate substrate can greatly improve the intensity of Raman signal and is more conducive to the diagnosis of tumors. Therefore, SERS based tumor diagnosis is more suitable for detection of samples with low concentration, such as the detection of tumor biomarkers. Since the SERS substrates greatly improve the intensity of Raman signal, the data processing of SERS spectrum was relatively simple. The conventional methods mainly utilize peak intensity comparison and multivariate statistical analysis. Meanwhile, artificial intelligence methods are also being used to improve diagnosis accuracy. In this chapter, we first introduce the conventional procedure in tumor diagnosis based on SERS, and then introduce on the AI application in tumor diagnosis.

Conventional procedure

The conventional procedure for tumor diagnosis based on SERS necessitates (i) sample preparation and nanoparticles (NPs) preparation; (ii) spectral acquisition; (iii) data processing and analysis. The first step of the preparation process is mainly divided into sample preparation and nanoparticle preparation. After preparation, the Raman microscope would collect the Raman spectroscopy from the preprocessing samples. Then, theses Raman spectra would be processing and analysis for tumor diagnosis, for example, bladder cancer [111–113], brain cancer [114–116], breast cancer [117–126], cervical cancer [127], gastric cancer [128], liver cancer [129–132], lung cancer [133, 134], melanoma [135, 136], nasopharyngeal cancer [137], osteosarcoma [138], pancreatic cancer [139], prostate cancer [140–142], salivary gland neoplastic [143], thyroid cancer [144] (Table 3).

For samples preparation, tissue [114] or tissue homogenates [115, 143] have been relatively less studied as samples unlike conventional Raman spectroscopy diagnostic methods. Besides, it is difficult to gain the tumor tissues via traditional biopsies repeatedly for analysis. Therefore, body fluids, easily accessible samples, are widely

Table 3 SERS for tumor diagnosis

Sample	Target	Substrates	Methods	LOD	Diagnosis	Ref
Tissue	-	Ag NPs@Ag NR	PCA	5.0×10^{-9} M	Brain cancer	[114]
Tissue homogenate	-	Ag films	PCA	-	Brain cancer	[115]
	-	Ag films	PLS, PCA	-		[116]
	-	Ag films	PCA, PLS-DA	-	Salivary glands carcinoma	[143]
Cell	mRNA	Au nanoclusters	-	3.4 pM	Bladder cancer	[111]
	miRNA	Ag nanopillar	-	451 zmol, 1.65 amol	Breast cancer	[117]
	Creatinine	Ag NRs	PCA, PLS-DA	5.3 μM		[118]
	miRNA	Au NPs	-	-		[119]
	miRNA	Au NPs	-	1 pmol/L		[121]
	EGFR	TiO_x	-	1 nM		[124]
	Exosome	Au NRs	-	5.3×10^3 particles/mL		[125]
	-	Au NP colloid	PCA-LDA	-	Breast esophageal & liver cancer	[145]
	CSCs	Ni-based nanoprobes	PCA	-	Breast cervical & lung cancer	[146]
	VEGF	Fe_3O_4/Au NPs	-	2.3 pg/mL	Melanoma	[135]
	CTCs	Au NPs	-	-		[136]
	Telomerase	Au NPs	-	-	Lung cancer	[147]
Blood	CTCs	Au-rGO@anti-ErbB2	-	5 cells/mL	Breast cancer	[120]
	CTCs	TiO_2 NPs	-	2 cells/mL		[126]
	CTCs	Au NPs	-	-	Liver cancer	[131]
	CTCs	Ag_2O-4MPY-rBSA-FA	-	1 cell per mL		[132]
	MMPs	Au NPs	-	0.07 ng/mL	Nasopharyngeal cancer	[137]
Plasma	-	Ag NPs	PCA-LDA	-	Bladder cancer	[112]
	Exosome	Au NSs	-	2.4 particles/mL	Lung cancer	[134]
	Exosome	Au NPs	PCA	-	Osteosarcoma	[138]
	-	Ag NPs	PCA-LDA PLS-DA		Thyroid tumors	[144]
Serum	-	Ag NPs	PCA-QDA		Gastrointestinal tumors	[128]
	Albumin	Ag colloid	PCA-LDA	-	Liver cancer	[129]
	AFP	Au@AgNCs/MoS_2	-	0.03 pg /mL		[130]
	-	Ag NPs	PCA-LDA	-	Prostate cancer	[140]
	AR-V7 protein	Au films	-	16 μg/ mL		[141]
	PSA	Au NPs	-	0.9 pg/mL		[142]
Urine	mRNA	Au nanoclusters	-	3.4 pM	Bladder cancer	[111]
	-	Ag colloid	PCA-LDA	-		[113]
Tear	-	Au/HCP-PS	PCA-LDA	-	Breast cancer	[122]
Exhaled breath	Aldehydes	Ag NPs@ZIF-67/g-C_3N_4	-	1.35 nM	Lung cancer	[133]
Biomarker solution	EpCAM, CEA	Ag nanoforest	-	0.2 pmol	Colorectal cancer	[148]

Table 3 (continued)

Sample	Target	Substrates	Methods	LOD	Diagnosis	Ref
Cell	CTCs	Ag layer	KNN	-	Breast cervical laryngeal liver lung ovarian cancer	[149]
	-	Ag layer	SVM	-	Lung cancer	[150]
	EVs	Au nanohole	LR	-	Ovarian cancer	[151]
Serum	-	Au NPs	PCA-SVM	-	Cervical & breast cancer	[123]
	-	ZnO/AgNP/AuNP	1D-CNN	-	Liver cancer	[152]
	EVs	Au-CD81-EVs-EphA2-Au	CT	-	Pancreatic cancer	[153]
Urine	-	Ag colloid	SVM	-	Liver cancer	[154]

CSCs Cancer stem cells, *CEA* Carcinoembryonic antigen, *CTCs* Circulating tumor cells, *CT* Classification tree, *CNN* Convolutional neural network, *EGFR* Epidermal growth factor receptors, *EpCAM* Epithelial cell adhesion molecule, *EVs* Extracellular vesicles, *Au NRs* Gold nanorods, *Au NSs* Gold nanostars, *KNN* k-nearest neighbors, *LOD* Limit of detection, *LDA* Linear discriminate analysis, *LR* Logistic regression, *MMPs* Matrix metalloproteinases, *NCs* Nanocubes, *PLS* Partial least squares, *DA* Discriminate analysis, *PCA* Principal component analysis, *PSA* Prostate specific antigen, *QDA* Quadratic discriminant analysis, *Ag NPs* silver nanoparticles, *Ag NRs* silver nanorods, *SVM* Support-vector machines, *VEGF* Vascular endothelial growth factor, *AFP* α-fetoprotein

used to diagnose tumor, such as tears [122], serum [123, 128, 129, 140–142], plasma [112, 144], urine [113]. Since SERS can significantly improve the Raman signal intensity, researchers are more inclined to detect samples with finer scale. Cells are more delicate at the detection scale than tissues, so cell detection based on SERS can be used for cancer diagnosis, such as breast cancer cell [118, 145], hepatoma cell [145], esophageal cancer cell [145], bladder cancer cell [111].

In addition, tumor biomarkers, a non-invasive and rapid analysis, has recently demonstrated the potential to solve the limitations of conventional biopsy. Because of the low abundance and chemical complexity of these materials, SERS, a very excellent Raman enhancement technology, is appropriate for detection and analysis tumor biomarkers. Recently, several researches have conducted about tumor biomarkers by SERS, such as aldehydes in exhaled breath [133], carcinoembryonic antigen (CEA) [148], circulating tumor cells [120, 126, 131, 132, 136], epithelial cell adhesion molecule (EpCAM) [148], epidermal growth factor receptors (EGFR) [124], exosomes [125, 134, 138], matrix metalloproteinases (MMPs) [137], micro RNAs (miRNAs) [117, 119, 121], mRNA [111], p16/Ki-67 [127], prostate specific antigen [142], protein [130, 141]. In addition to tumor biomarkers, other biomolecules related to tumor growth and dissemination are also detected by SRES technology to monitor or diagnose tumor changes, for example, cancer stem cells [146], cell lysates [118], proteases [137], telomerase [147], vascular endothelial growth factor [135].

For nanoparticles preparation, noble metal NPs are the mostly applied for tumor diagnosis with the advantages of low cost and easy synthesis, such as Au [111, 119–123, 125, 131, 134–137, 141, 142, 145, 147], Ag [112–115, 117, 118, 127–129, 132, 133, 140, 143, 144, 148, 155], where the single metal as the original nanoparticle (Fig. 5a, b). However, the single SERS nanoparticle has its own shortcomings, the bimetallic nanoparticle substrate such as Au@Ag [130] combines the advantages of two metals
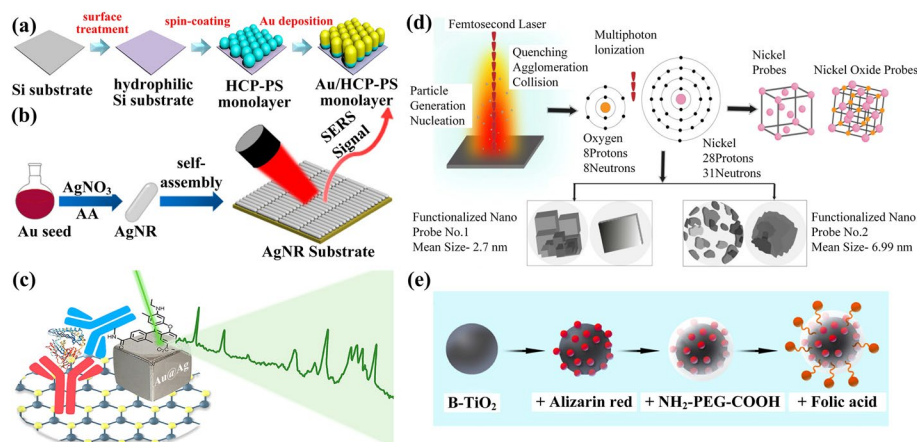
Fig. 5 SERS substrate **a** Au substrate [122]; **b** Ag substrate [118]; **c** Au@Ag substrate [130]; **d** Ni substrate [146]; **e** TiO$_2$ substrate [126]

(Fig. 5c), which maybe have better SERS enhancement effect. Except these noble metals (Au/Ag), other transition metals such as Ni [146] also produce an enhanced effect and have been applied for tumor diagnosis (Fig. 5d). Oxide semiconductors such as TiO$_2$ [124, 126] also have a SERS enhanced effect and have been utilized for detecting the cancer biomarkers (Fig. 5e).

After sample preparation and nanoparticle preparation, the Raman spectroscopy acquisition will be the next step. Compared with the spontaneous Raman signal intensity, SERS greatly improved the Raman signal intensity, so commercial Raman spectrometers could be directly used in the process of Raman spectroscopy data acquisition. At the same time, some miniaturized Raman spectrometers, such as hand-held Raman spectrometers [148] or portable Raman spectrometers [122, 128, 133, 147], can be used for signal acquisition because the Raman signal has been greatly improved, which can better achieve a fast, flexible, and convenient acquisition process.

Data processing and analysis is the final and vital step for tumor diagnosis by SERS, which can be divided into two types: detection of biomarkers or biomolecules and diagnosis classification. The limit of detection (LOD) is used to evaluate the detection ability of the former, while the accuracy, sensitivity and specificity to demonstrate the classification capacity of the latter. At the same time, the limit of quantification (LOQ) can also be used for evaluate the detection ability of the detection of biomarkers or biomolecules [118]. Moreover, several researches can simultaneously achieve the detection of biomarkers and diagnosis of cancer [118].

For detecting the biomarkers biomolecules, the LOD of circulating tumor cells (CTCs) in the peripheral blood of cancer patients could reach 1 cell per mL [132], 2 cells/mL [126], up to 5 cells per mL [120]. The LOD of two miRNA markers for breast cancer (miR-21 and miR-155) was 451 zmol and 1.65 amol respectively [117],while the LOD of exosomal miRNA reaching as low as 1 pmol/L [121]. The LOD of mRNA for detection of bladder tumor could extend 3.4 pM [111]. The LOD of exosomes can achieve the detection limit of 2.4×10^3 particles/mL [134], 5.3×10^3 particles/mL [125]. Furthermore, Kim et al. [148] successfully detected the cancer biomarkers (EpCAM, CEA) in tiny amount

of sample solutions (∼2 μl) with as low as 0.2 pmol of the protein biomarkers. Er et al. [130] developed a SERS immunosensor and exhibited a wide linear detection range (1 pg/mL to 10 ng/mL) with a LOD as low as 0.03 pg/mL toward α-fetoprotein with good reproducibility and stability. Lin et al. [137] have designed the metal carbonyl nanobarcodes for detecting MMPs with strong sensitivity (LOD 0.07 ng/mL). Turan et al. [142] introduced a novel designed sensor for detection of prostate specific antigen with the LOD and LOQ of 0.9 pg/mL and 3.2 pg/mL, respectively. Keshavarz et al. [124] achieved semiconductor materials (TiO_X) as a SERS template to diagnose breast cancer with the LOD of 1 nM. Huang et al. [133] successfully achieved the ultrasensitive detection of aldehydes in exhaled breath of lung cancer patients with a LOD 1.35 nM. Liu et al. [118] yielded a high sensitivity for the detection of creatinine with a low LOD of 5.3 μM and a LOQ of 17.68 μM. Huang et al. [135] traced vascular endothelial growth factor (VEGF) in cell lysis samples with an excellent limit of detection of 2.3 pg/mL under the optimum conditions.

For tumor diagnosis classification based on SERS, statistical analysis methods are usually used to analyze spectral differences and achieve the tumor diagnosis, which is the same as the conventional method for tumor diagnosis classification based on Raman spectroscopy. The multivariate statistical analysis methods contain PCA [114, 115, 138], PCA-LDA [112, 113, 122, 129, 140, 144, 145], PLS [116], PLS-DA [143], PCA-QDA [128]. Among using PCA method, Kowalska et al. [115] proved that tumor brain samples can be discriminated well from the healthy tissues by using only three main principal components with 96% of accuracy, while Li et al. [114] reported that healthy brain tissue and Grade II gliomas as low grade gliomas as well as Grade III and Grade IV as high-grade gliomas can be clearly distinguished by three-dimensional PCA. Moreover, Han et al. [138] identified the osteosarcoma by combining SERS and matrix-assisted laser desorption/ionization time-of-flight mass spectrometry profiling of exosomes with all 100% sensitivity, specificity, and accuracy. Among PCA-LDA method, Hu et al. [113] utilized SERS for detecting urine metabolites of bladder cancer with the total diagnostic sensitivity and specificity 100% and 98.85%, respectively, while Qian et al. [112] utilized SERS of pretreated plasma samples to predict disease recurrence in muscle-invasive bladder cancer patients undergoing neoadjuvant chemotherapy and radical cystectomy revealing a high accuracy of 85.2% in prediction of disease recurrence. Especially for determination of cancer stages, Gao et al. [129] screened liver cancer (LC) at different tumor (T) stages by serum albumin, in conjunction with SERS and finally classified the early T (T1) stage LC vs. normal group and advanced T (T2–T4) stage LC vs. normal group, yielding high diagnostic accuracies of 90.00% and 96.55%, respectively by PCA-LDA method. For PLS/PLS-DA method, Kowalska et al. [116] reported that the differentiation between primary and secondary brain tumors SERS data was completed PLS method with a very high 85% of accuracy, while Czaplicka et al. [143] analyzed salivary glands carcinoma, tumor and healthy tissues and their homogenates by SERS and PLS-DA method, showing correlation accuracy as 0.98 with sensitivity 0.97, and specificity 0.89. In addition, Avram et al. [128] utilized PCA-QDA method for classifying gastrointestinal tumors by different testing models, where the results showed that the classification accuracy yielded by combining SERS analysis of serum with C-reactive protein levels, neutrophil counts, platelet counts and hemoglobin levels was superior (accuracy

83.33%) to the classification accuracy yielded by SERS profiling alone (accuracy 76.92%) and to the one yielded by blood tests (accuracy 73.08%). In a word, multivariable statistical analysis methods are commonly used with spectral data processing, no matter the tumor diagnosis method based on Raman spectroscopy or the tumor diagnosis method based on SERS. Similarly, AI methods, as a complement to conventional methods, will serve as a superior method to improve the accuracy of tumor diagnosis.

AI application

Since SERS can greatly improve the detection signal of samples, the tumor diagnosis methods based on SERS are mostly used for the detection of small molecules such as cells and biomarkers, resulting in the collected Raman signal processing often used for the calibration of detection limits. Of course, some Raman signals are used for classification diagnosis, where researchers usually utilized multivariate statistical methods for classification. Even so, artificial intelligence methods also provide unique methods for classification diagnosis to improve accuracy, such as breast cancer [123, 149], liver cancer [152, 154], lung cancer [150], ovarian cancer [151], pancreatic cancer [153] (Table 3).

For typical ML methods, SVM is the most widely used method for classification. Dawuti et al. [154] utilized urine SERS combined with SVM method to identify liver cirrhosis (sensitivity 88.9%, specificity 83.3%, and accuracy 85.9%) and hepatocellular carcinoma (sensitivity 85.5%, specificity 84.0%, and accuracy 84.8%), while Fang et al. [150] also implemented SERS technique combined with SVM to identify and distinguish non-small-cell lung cancer (NSCLC) and small cell lung cancer (SCLC) cells from normal cells including blood cells and immortalized lung cells, where achieving the classification accuracy of 98.8% between NSCLC cells and normal cells and reaching the accuracy 100% in the classification of SCLC cells and normal cells, as well as SCLC cells and NSCLC cells (Fig. 6a). Except SVM method, Banaei et al. [153] applied the classification tree method to the analysis of the expression level of EVs biomarkers in pancreatic cancer, chronic pancreatitis, and normal controls individuals, measuring the sensitivity and specificity as 0.95 and 0.96, respectively (Fig. 6b). Moreover, Ćulum et al. [151] discriminated the EVs isolated from different ovarian cancer cell lines by a logistic regression-based machine learning method with ~99% accuracy, sensitivity, and specificity.

Deep learning is an advanced machine learning method that can be used to discriminate various data accurately. Furthermore, deep learning has been applied for tumor diagnosis based on SERS. Fang et al. [149] utilized the feature peak ratio method, PCA combined with KNN, and residual network to classify the SERS spectra from blood cells and tumor cells. The results show that the ratio method and PCA combined with the KNN could only identify some tumor cells from blood cells, but residual network method could quickly distinguish various tumor cells and blood cells with an accuracy of 100% (Fig. 6c). This indicates that deep learning has great potential in tumor classification and diagnosis. In addition, Cheng et al. [152] constructed a convolutional neural network classifier for recognizing serum SERS spectra as deep learning inputs. The 1D-CNN method achieved a prediction accuracy of 97.78% on an independent test dataset randomly sampled from normal controls, hepatocellular carcinoma cases, and hepatitis B patients (Fig. 6d).
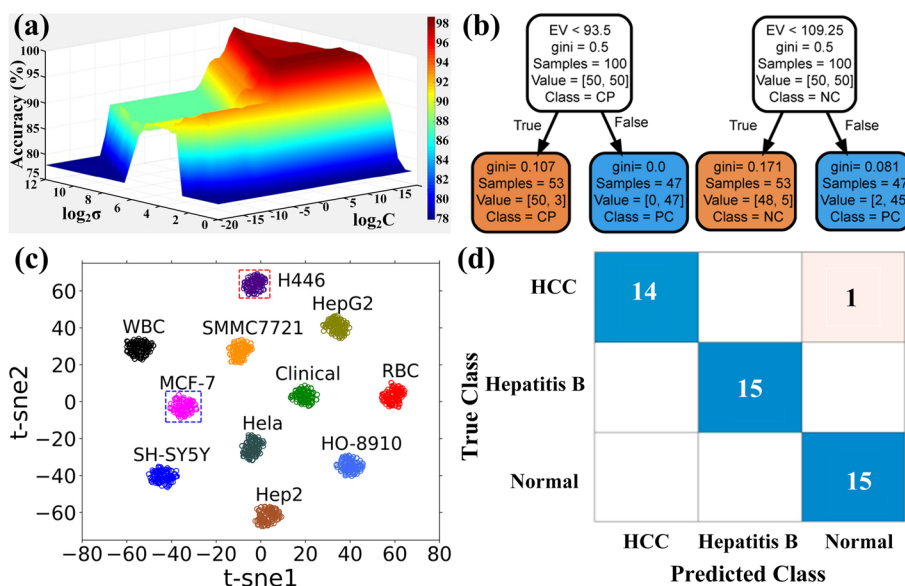
Fig. 6 AI method for tumor diagnosis by SERS **a** 3D map of classification accuracy for the SVM model [150]; **b** The classification tree analysis of the expression level of EVs biomarkers [153]; **c** Residual network classification results of various tumor cells and blood cells [149]; **d** CNN classifier results of the independent test dataset for recognizing serum SERS spectra [152]

In conclusion, the key of tumor diagnosis based on SERS is to find suitable enhanced nanoparticle substrates so as to greatly increase the original Raman signal. Since the original Raman signal is weak, the differences between normal and cancerous samples will become larger after enhancement. Therefore, the exploration of detection limit is a very important aspect in tumor diagnosis based on SERS. Otherwise, due to the signal enhancement brought by SERS technology, the data processing of tumor classification and diagnosis based on SERS is easier, and multivariate statistical method is often used to distinguish. However, despite the multivariate statistical methods have achieved a high classification accuracy, but from the data processing process of tumor diagnosis methods based on SERS, the classification accuracy still can be improved, especially when artificial intelligence method is used for data processing and classification, which has been proved by some literatures. Whereas, there is still relatively little literature on these diagnostic methods using artificial intelligence [70, 76]. In the future, tumor diagnosis based on SERS should start from two aspects: signal enhancement and classification diagnosis. On the one side, more suitable SERS substrates with greater signal intensity increased should be sought from the perspectives of biocompatibility and spatial distribution. On the other side, for tumor classification, new data processing methods such as artificial intelligence can be selected to provide the accuracy of classification and diagnosis.

Raman imaging for tumor diagnosis

Raman imaging can obtain more information, so it has broad application potential in tumor diagnosis. The processing of Raman figure is the most important part of this method. Compared with spectral data, Raman images carry more information. Therefore, in the processing of Raman images, the conventional method is to directly carry

out comparative analysis of images, or adopt multivariate statistical analysis method, which is feasible for small-batch images. But when faced with a large number of images, this method is time consuming. As an automatic method of image analysis, processing and mining, artificial intelligence has important application value in tumor diagnosis based on Raman imaging. In this chapter, we first introduce the conventional procedure in tumor diagnosis based on Raman imaging, and then focus on the AI application in tumor diagnosis.

Conventional procedure

The conventional procedure for tumor diagnosis based on Raman imaging contains (i) sample preparation; (ii) image acquisition; (iii) image processing and analysis. Tissues are the most applied materials for Raman imaging, as well as cells. Due to weak scattering effect, measurements of spontaneous Raman spectra with a competent signal to noise ratio can be time-consuming [156]. Therefore, conventional Raman spectroscopy measurements are limited to smaller sample areas. For large scale sample, nonlinear optical technologies (coherent anti-Stokes Raman scattering; stimulated Raman scattering) have shown success in tissue and cell imaging for tumor diagnosis [157–159]. After collecting the Raman imaging, it is vital for image processing with suitable methods. Comparative analysis of Raman images is the most direct method, but it is for small-scale data volume. When the amount of data is huge, artificial intelligence is often used for analysis and diagnosis, which has achieved a very high diagnostic performance. At present, multiple types of tumor samples have been accurately diagnosed based on Raman imaging, such as benign cementoma [160], bladder cancer [161, 162], brain cancer [163–165], breast cancer [163, 166–168], chondrogenic tumor [169], colorectal cancer [59, 170], glioma [171], meningiomas [172], prostate cancer [156, 173, 174], spine tumors [164], skin cancer [175], skull base tumors [176, 177] (Table 4). In addition to diagnosing tumors directly, Raman imaging can also capture the components or metabolites, such as glycogen [178], lipid droplets [179], in cells to analyze the differences and changes between normal cells and cancer cells, thus playing a role in monitoring the cancer progression and tumorigenesis.

For sample preparation, tissue is the most common source of samples, especially fresh, unprocessed biological tissues. Cordero et al. [161] utilized the entire extracted biopsy without thin-sectioning to characterize the tumor grading ex vivo, using a compact fiber probe-based Raman imaging system. Liao et al. [167] used the adipose tissue in breast resections to assess the surgical margins by high wavenumber Raman imaging and fingerprint Raman spectroscopy, which can reduce the overall tissue analysis time and maintain high diagnostic accuracy. Boitor et al. [180] presented a prototype device based on integrated auto-fluorescence imaging and Raman spectroscopy for intraoperative assessment of surgical margins during Mohs micrographic surgery of basal cell carcinoma (BCC), and the results showed that typically more than 95% of the resection area is analyzed by the Fast Raman device, which includes both the epidermal and deep margin, without requiring tissue trimming (Fig. 7a). In addition to imaging from fresh, untreated biological tissue, it is also able to image unstained tissue after sectioning. D'Acunto et al. [169] utilized the 5 μm unstained tissue specimens for Raman imaging to the diagnosis and grading of chondrogenic

Table 4 Raman imaging for tumor diagnosis

Sample	Target	Technology	Method	Diagnosis	Ref
Tissue	-	CRM	Peak comparison	Benign cementoma	[160]
	-		PLS-DA	Bladder cancer	[161]
	HAp		PCA	Breast cancer	[166]
	-		-		[167]
	-		-	Chondrogenic Tumors	[169]
	-		Peak comparison	Colon cancer	[170]
	-		-	Skin cancer	[175]
	-		SVM		[180]
	-	SRH	Cohen's kappa	Brain & spine tumors	[164]
	-		-		[165]
	-		Cohen's kappa	Glioma	[171]
	-		Cohen's kappa	Meningiomas	[172]
	-		Cohen's kappa	Sinonasal & skull base tumors	[176]
	-		Cohen's kappa	Skull base tumors	[177]
	-		-	Central nervous system lesions	[181]
	-	LSRM	PCA-SVM	Pituitary adenomas	[182]
Cell	-	CRM	PCA, PLS-DA	Bladder cancer cells	[162]
	-		RF	Breast cancer cells	[168]
	EVs		-		[183]
	Fatty acid		-	Cervical cancer cells	[184]
	Vitamin C		Peak comparison	Colorectal cancer cells	[59]
	Lipids		-	Endothelial cells	[185]
	Retinol		-	Glioblastoma cancer cells	[186]
	Cholesteryl esters		-	Prostate cancer cells	[156]
	-		PCA		[173]
	LDs		-		[174]
	LDs	SRS	-	Breast cancer cell	[187]
	-		-	Cervical cancer cell	[188]
	Ponatinib		-	Leukemia cell	[189]
	Glycogen		-	Melanoma cell	[178]
	LDs		-		[179]
	-		-	Pancreatic cancer cell	[190]
	Telomerase, microRNA	SERS	-	Breast & cervical cancer cells	[191]
	Exosomes		-	Cervical cancer cell	[192]
	-		-		[193]
	-		-	Colon cancer cell	[194]
	Membrane receptor		-		[195]
	-		-	Glioblastoma cells	[196]
Tissue	-	SRS	SVM	Glioblastomas	[197]
	Calcifications		SVM	Breast tumor	[198]
	-	SRH	CNN	Brain tumor	[31]
	-		CNN		[199]
	Cell		CNN		[200]
	-		CNN	Gastric cancer	[201]
	-		CNN	Glioma	[202]
	-		CNN	Laryngeal carcinoma	[203]

CRM Confocal Raman microscope, *CNN* Convolutional neural network, *EVs* Extracellular vesicles, *HAp* Hydroxyapatite, *LSRM* Line scan Raman microspectroscopy, *LDs* Lipid droplets, *PLS* Partial least squares, *DA* Discriminate analysis, *PCA* Principal component analysis, *RF* Random forest, *SERS* Surface-enhanced Raman spectroscopy, *SRH* Stimulated Raman histology, *SRS* Stimulated Raman scattering, *SVM* Support-vector machines
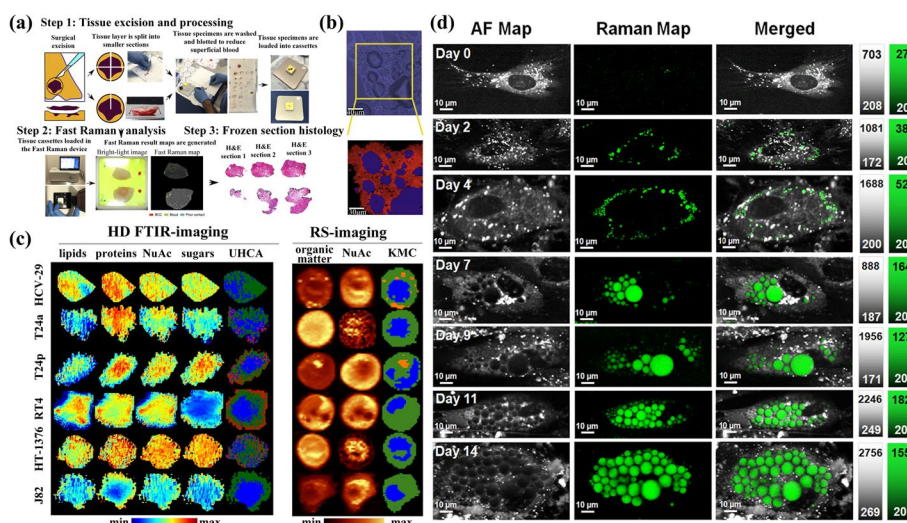
Fig. 7 Conventional method for tumor diagnosis by Raman imaging **a** Integration of the Fast Raman device in the pathway of Mohs surgery [180]; **b** The microscopy image and Raman image of noncancerous sigmoid colon mucosa tissue [170]; **c** FTIR and RS images of cells [162]; **d** AF mapping images and Raman mapping images of live adipocytes at the time of differentiation [204]

tumors, including enchondroma and chondrosarcomas of increasing histologic grades. Brozek-Pluska et al. [170] applied 16 μm sections from the nonfixed, fresh samples to differentiate noncancerous and cancerous human sigmoid colon mucosa based on Raman spectroscopy and imaging (Fig. 7b). Feng et al. [175] adopted the skin sections of 20 μm thickness for rapid discrimination of basal cell carcinoma tumor by a superpixel acquisition approach, which expedited acquisition with two to five orders of magnitude faster than conventional point-by-point scanning by trading off spatial resolution.

Cells, as a much minute scale of observation than tissue, show more subtle signs of changes in the tumor. Therefore, Raman imaging of the cells can more clearly find the changes on the cellular scale of the tumor. Kujdowicz et al. [162] employed Fourier transform infrared (FTIR) and Raman spectroscopic (RS) imaging to investigate bladder cancer cell lines of various invasiveness, and demonstrated that FTIR and Raman spectroscopy can be employed to distinguish between different bladder cancer cells of various malignancy (Fig. 7c). Beton et al. [59] evaluated the biochemical and structural features of human colon cell lines based on Raman spectroscopy and imaging, and shown that normal reactive oxygen species-injured and cancerous human colon cells could be distinguished based on their unique vibrational properties. Paidi et al. [168] utilized 3D optical diffraction tomography and Raman spectroscopy for optical phenotyping of cancer cells at single-cell resolution, and demonstrated that coarse Raman microscopy is capable of rapidly mapping a sufficient number of cells for training a classifier that can accurately predict the metastatic potential of cells at a single-cell level.

Cell imaging based on Raman spectroscopy, not only can be used to image the cellular morphology, but also can be used to image the cell cytosolic microstructures, to achieve subcellular level analysis of the components of cancer cells. Roman et al. [174]

leveraged the Raman mapping technique to investigate lipid droplets (LDs) composition in untreated and irradiated with X-ray beams prostate cancer cells, proved lipids accumulation in PC-3 cells by Raman mapping technique, and revealed the heterogeneous composition of LDs. Suhito et al. [204] reported a novel optical method called "autofluorescence-Raman mapping integration (ARMI)", which used cell autofluorescence to reveal cellular morphology and cytosolic microstructures, while Raman mapping allowed site-specific intensive analysis of target molecules, which enables ultra-fast identification of cell types. The novel technique has rapidly and precisely analyzed the adipogenesis (Fig. 8d). Abramczyk et al. [186] utilized the Raman imaging to detect molecular processes that occur in normal and cancer brain cells due to retinol transport in human cancers at the level of isolated organelles and found that aberrant expression of retinoids and retinol binding proteins in human tumors could be localized in lipid droplets, and mitochondria. Uematsu et al. [184] presented a new method for simultaneously visualizing up to five atomically labeled intracellular fatty acid species by Raman imaging and revealed that fatty acids with more double bonds tend to concentrate more efficiently at lipid droplets. Radwan et al. [185] considered the astaxanthin as a new Raman probe for the detection of lipids in the endothelial cells of various vascular beds, where the astaxanthin colocalized with lipids in cells could enable Raman imaging of lipid-rich cellular components with lower laser power. Horgan et al. [183] presented a new strategy for simultaneous quantitative in vitro imaging and molecular characterization of EVs in 2D and 3D based on Raman spectroscopy and metabolic labelling, and showed that metabolic deuterium incorporation demonstrated no apparent adverse effects on EV secretion, marker expression, morphology, or global composition.

For the Raman imaging, spontaneous Raman spectroscopy gives an opportunity to investigate biochemical changes in biological samples [59, 161, 162, 167−170, 174, 175,
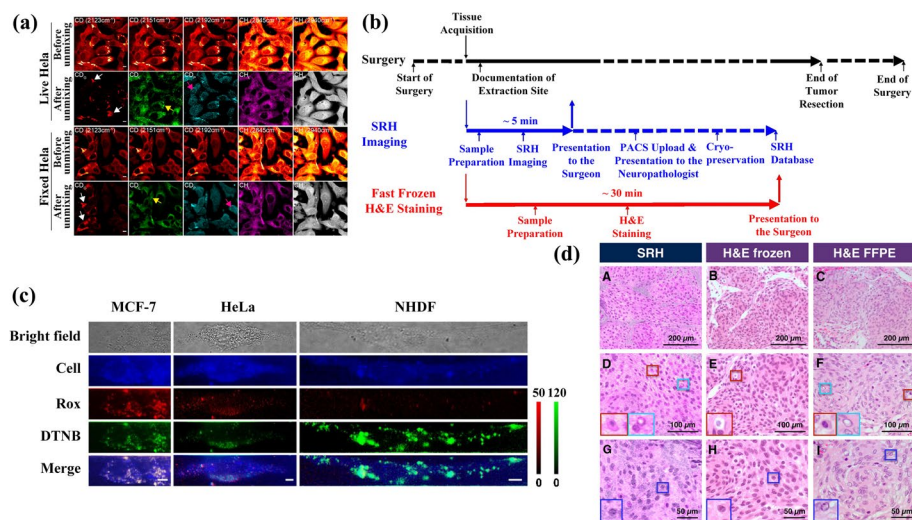

Fig. 8 SRS/SRH/SERS method for tumor diagnosis by Raman imaging **a** SRS imaging of different components in live and fixed HeLa cells after culturing in d7-glucose medium [178]; **b** Workflow of SRH imaging in neurosurgery [165]; **c** Raman imaging of MCF-7, HeLa and NHDF cells treated with Au NPs-H2 and end assembly [191]; **d** Comparison of cellular features available with SRH versus conventional H&E stained slides in representative case of Meningioma [177]

183–186, 204]. However, due to weak scattering effect and low resolution, spontaneous Raman imaging is limited to small area samples [156]. Therefore, Raman enhancement techniques are needed to provide signal strength to achieve higher resolution and imaging effects [205]. Stimulated Raman scattering (SRS) and surface enhanced Raman scattering have been applied for Raman signal amplifications to achieve tumor diagnosis.

SRS amplifies the weak spontaneous Raman signal via stimulated emission by orders of magnitude to enable fast imaging with molecular specificity inherited from spontaneous Raman spectroscopy [206]. Lee et al. [178] leveraged the stimulated Raman scattering microscopy with metabolic incorporation of deuterium-labeled glucose to visualize glycogen in live cancer cells (Fig. 8a), and characterized different glycogen metabolic phenotypes in a series of mutant melanoma cell lines by this method. Tipping et al. [187] demonstrated the multi-wavelength SRS imaging together with spectral phasor analysis to characterize a panel of breast cancer cell lines treated with two clinically relevant statins, and revealed the lipid droplet distribution throughout populations of live breast cancer cells by SRS imaging within the high wavenumber. Du et al. [179] utilized SRS of intracellular lipid droplets to identify a previously unknown susceptibility of lipid mono-unsaturation within dedifferentiated mesenchymal cells. Bae et al. [188] reported a unique spatial light-modulated stimulated Raman scattering microscopy to monitor real-time cancer treatment effects, and showed immediate apoptotic response when monitoring the therapeutic effect of mild alkaline solution on cancer cells. Sepp et al. [189] utilized the SRS to image label-free ponatinib in live human chronic myeloid leukemia cell lines with high sensitivity and specificity. Lin et al. [190] developed a deformable mirror-based remote-focusing SRS microscope, and performed volumetric chemical imaging of living cells.

Stimulated Raman histology, developed from SRS, utilizes the intrinsic vibrational properties of lipids, proteins and nucleic acids to generate image contrast, revealing diagnostic microscopic features and histologic findings poorly visualized with hematoxylin and eosin (H&E)-stained images, such as axons and lipid droplets [207], while eliminating the artifacts inherent in frozen or smear tissue preparations [208]. The SRH has shown great potential for rapid and accurate tumor diagnosis [201–203], demonstrating diagnosis in near-perfect agreement with conventional H&E [31, 164, 171, 172, 176, 177, 181]. Neidert et al. [165] established a dedicated workflow (Fig. 8b) for SRH serving as an intraoperative diagnostic, research, and quality control tool in the neurosurgical operating room, and suggested to optimize the process regarding tissue collection, preparation, and imaging during using this novel imaging modality for intraoperative diagnostic.

SERS enhances the Raman spectrum signal by plasmon resonance [20], and can also achieve Raman imaging for tumor diagnosis rather than acquiring the Raman spectra. Liu et al. [191] demonstrated a target-triggered regioselective assembly strategy of plasmonic nanoprobes for dual Raman imaging of intracellular cancer biomarkers, and successfully performed Raman imaging of MCF-7, HeLa and normal human dermal fibroblasts (NHDF) cells with this strategy(Fig. 8c). Chen et al. [192] designed an Ag SERS substrate to track of the intracellular distribution of exosomes and the concurrent quantitative sensing of environmental pH, and demonstrated that exosomes first attached with the tumor cell surfaces, and then entered into the cells and accumulated in lysosomes as time prolonged. Yuan et al. [194] reported a special nanoparticle which

can be detected with high specificity in furin-overexpressing tumor cells, and applied in high-resolution image-guided surgery to precisely delineate tumor margins during and after resection in real-time. Burgio et al. [196] achieved the stable and specifically targeting SERS tags for visualization of the exact tumor borders and infiltrating foci of glioblastoma through application of the appropriate gold nanoparticles surface chemistry and by the correct balance of inert and active targeting functionalities.

For image processing and analysis, picture comparison analysis and Raman peak intensity comparison is the intuitive and simple processing method. Abramczyk et al. [163] used Raman spectroscopy and Raman imaging to monitor changes in the redox state of the mitochondrial cytochromes in ex vivo human brain and breast tissues, and found that the concentration of reduced cytochrome c becomes abnormally high in human brain tumors and breast cancers and correlates with the grade of cancer. Furthermore, multivariate statistical methods can also be used for image processing and analysis. Marro et al. [166] reported the 3D biochemical analysis of breast cancer microcalcifications, combining 3D Raman spectroscopy imaging and advanced multivariate analysis for investigating the molecular composition of HAp calcifications found in breast cancer tissue biopsies.

In particular, SRH is a novel technology that leverages laser spectroscopy and color-matching algorithms to create images similar to the formalin-fixed paraffin-embedded section [176]. The key to SRH analysis and diagnosis lies in the consistency between SRH images and H&E sections. Fitzgerald et al. [176] assessed the time taken for results and diagnostic concordance between SRH images and FFPE section from the patients undergoing sinonasal and skull base surgery, and the results showed that the sensitivity, specificity, precision, and overall accuracy of SRH were 93.3%, 94.1%, 93.8%, and 93.3%, respectively, and near-perfect concordance was seen between SRH and frozen section with Cohen's kappa of 0.89. Pekmezci et al. [171] acquired glioma margin specimens for SRH, histology, and tumor specific tissue characterization, and the results yielded that consistency between immunohistochemistry (IHC) and SRH was near perfect with Cohen's kappa of 0.84 while the substantial agreement between IHC and H&E with Cohen's kappa of 0.67 and between SRH and H&E with Cohen's kappa of 0.72. Shin et al. [177] evaluated the skull base tumor diagnostic accuracy beyond cancer/non-cancer determination and neuropathologist confidence for SRH images contrasted to H&E-stained frozen and FFPE tissue sections (Fig. 8d), and the results revealed that SRH was effective for establishing a diagnosis using fresh tissue in most cases with 87% accuracy relative to H&E-stained FFPE sections. Straehle et al. [164] found a substantial diagnostic correlation between SRH-based neuropathological diagnosis and H&E-stained frozen sections ($\kappa = 0.8$), and the results showed that when diagnosing the brain and spine tumors, the accuracy of neuropathological diagnosis based on SRH images was 87.7% and was non-inferior to the current standard of fast frozen H&E-stained Sects. (87.3 vs. 88.9%). Di et al. [172] compared the diagnostic time and accuracy of SRH images with the gold standard (frozen section), and results revealed that the mean time-to-diagnosis was significantly shorter for SRH-mediated diagnosis compared with frozen Sect. (9.2 vs. 35.8 min), and the diagnostic accuracy was not significantly different between methods. Einstein et al. [181] explored the non-inferiority of SRH as compared to frozen section on the same piece of tissue in neurosurgical patients, and the results showed that

SRH was sufficient for diagnosis in 78% of specimens as compared to 94% of specimens by frozen section of the same specimen. In a word, SRH images shows a high degree of consistency with H&E staining sections, which provides an important prerequisite for rapid diagnosis using SRH. However, manual diagnosis of SRH images would undoubtedly increase the diagnosis time. Therefore, artificial intelligence methods should be sought to diagnose SRH images to reduce the diagnosis time, so as to truly apply SRH diagnosis to intraoperative diagnosis.

AI application

Images, as two-dimensional data, are more suitable as the input of artificial intelligence models. Therefore, artificial intelligence has great significance application in tumor diagnosis based on Raman imaging, whether using classical artificial intelligence method or the deep learning method. At present, Raman imaging based on artificial intelligence has been applied to a variety of tumor types, such as brain cancer [31, 197, 199, 202], breast cancer [198], gastric cancer [201], laryngeal cancer [203], prostate cancer [209] (Table 4).

For typical ML methods, SVM is a commonly used method for tumor diagnosis. Bae et al. [197] applied the hyperspectral SRS microscopy combined with SVM method for assessment of glioblastoma intertumoral heterogeneity (Fig. 9a), and found that the predominant proportion of glioblastoma tissue was consistent with the diagnosis from genomic analysis, but a significant portion of the remaining SRS image blocks in the specimens belonged to other molecular subtypes, implying a large degree of heterogeneity in glioblastoma. Yang et al. [198] leveraged hyperspectral SRS microscopy to evaluate the breast tumor malignancy based on tissue calcifications, and reached a precision of 98.21% and recall of 100.00% for classifying benign and malignant cases by using SVM method, significantly improving from the pure spectroscopy or imaging based methods. Doherty et al. [209] utilized the multimodal approach of Raman chemical imaging (RCI) and digital histopathology to image the prostate cancer tissues, then the multimodal approach achieved a sensitivity of 73.8% and specificity of 88.1% for Gleason grade 3/4 classification by SVM method.

Deep learning, as a machine learning method for large-scale image processing, has great application value in tumor diagnosis based on Raman imaging, especially the SRH combined with deep learning for tumor diagnosis. Group Orringer is the pioneer and leader of this diagnosis pattern. They reported a parallel workflow that combines SRH and deep convolutional neural networks to predict brain tumor diagnosis in near real-time in an automated fashion, where after training on over 2.5 million SRH images in their CNN, the workflow could predict brain tumor diagnosis in the operating room in under 150 s, an order of magnitude faster than conventional techniques (for example, 20 ~ 30 min) [31]. This amazing work shows the great potential for near real-time intraoperative diagnosis, which streamlines the workflow of intraoperative cancer diagnosis and creates a complementary pathway for tissue diagnosis that is independent of a traditional pathology laboratory. Moreover, they also utilized the SRH and deep neural networks to improve the intraoperative detection of glioma recurrence, and achieved a diagnostic accuracy of 95.8% when facing the external SRH validation dataset [202]. Except the wonderful work of Group Orringer, the Group Ji also recently yielded the
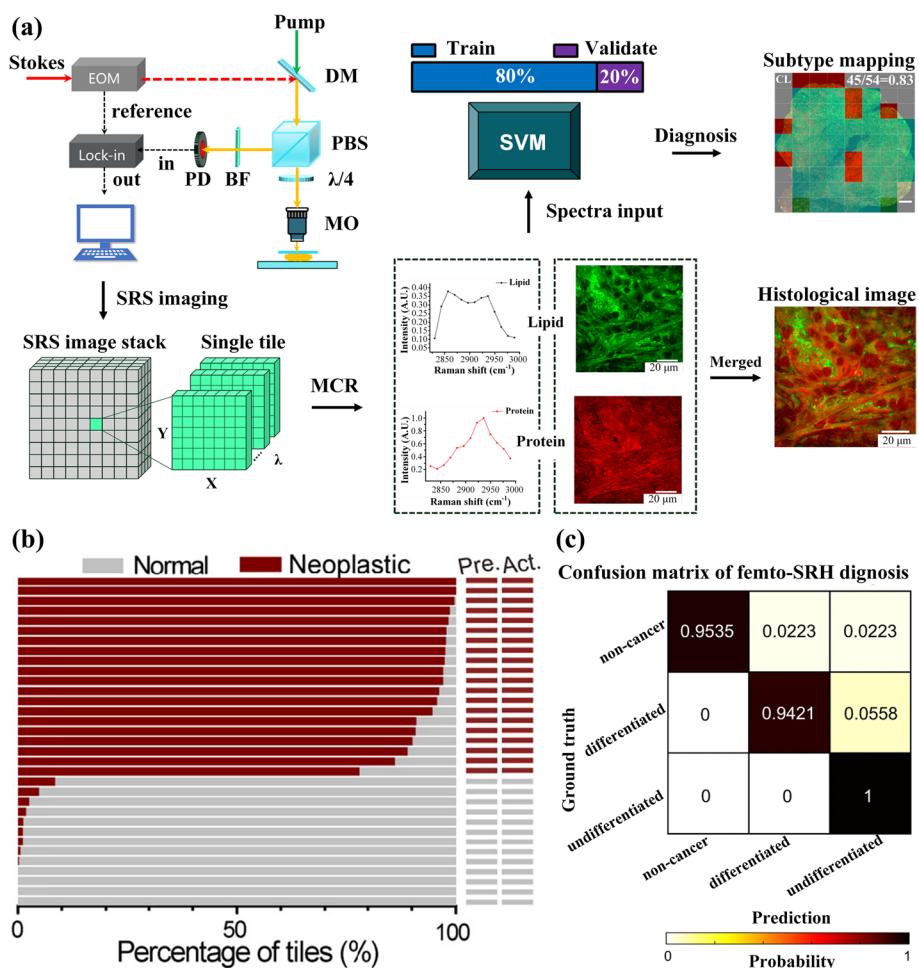
Fig. 9 AI method for tumor diagnosis by Raman imaging **a** Schematic illustration of the SRS imaging diagnostic platform for rapid glioblastoma subtyping by SVM method [197]; **b** Diagnostic results of 33 independent cases using residual network [203]; **c** Confusion matrix of the three diagnostic subtypes [201]

excellent advances in SRH combined with deep learning for tumor diagnosis. They applied this important pattern to diagnose the laryngeal squamous cell carcinoma on fresh, unprocessed surgical specimens, where they demonstrated near-perfect diagnostic concordance ($\kappa > 0.90$) between SRS and standard histology, and yielded the 100% accuracy of classifying 33 independent surgical specimens using deep-learning based SRS [203] (Fig. 9b). Furthermore, they recently leveraged the single-shot femtosecond SRS to reach the maximum speed and sensitivity with preserved chemical resolution, achieved < 60 s imaging the Fresh gastroscopic biopsy, and harvested the accuracy > 96% of predicting gastric cancer by CNN [201] (Fig. 9c).

In a word, Raman imaging has a wide application space in tumor diagnosis, because imaging can not only display the morphology of cells, but also show the distribution of cell components by using the vibration of special bonds. However, tumor diagnosis based on Raman imaging still has some problems such as imaging speed and resolution.

Therefore, tumor diagnosis based on Raman imaging can be improved from the following two aspects: One for Raman imaging technology. New Raman imaging techniques

can be explored to improve the resolution and speed of imaging. At the same time, new Raman enhancement techniques can also be explored to enhance weak signals so as to achieve more detailed imaging of cells or tissues. The other for imaging processing method. In terms of diagnosis, more excellent image processing methods can be applied, such as artificial intelligence methods, especially when SRH technology is used, which will greatly improve the efficiency of diagnosis and have high accuracy.

Conclusion, challenges and outlook

Tumor ranks as a leading cause of death and an important barrier to increasing life expectancy in each country of the world. In view of the problems of the current tumor detection methods, it is urgent to develop tumor diagnosis technology with intelligent attributes. According to recent studies, it is shown that Raman spectroscopy, as a label-free optical technique, has attracted more and more attention in tumor diagnosis, especially the Raman spectroscopy technique combined with AI. Here in this section, we compare and analyze firstly the three methods from sample acquisition, data collection and data processing, and give the clinical application direction of the three methods (Table 5). Then, we briefly discuss the challenges in in tumor diagnosis based on Raman spectroscopy, SERS, and Raman imaging, and the outlook of the future of AI for spectroscopic application.

For the acquisition of samples, tissues, cells, body fluids, and other kinds of specimens can be used to collect the Raman signals for tumor diagnosis. Conventional Raman spectroscopy and imaging methods can directly collect signals from samples, so as to achieve nondestructive testing. Compared with the other two methods, SERS need add the substrate as one more step, where the SERS substrate can greatly enhance the Raman

Table 5 The comparison of three methods

Method	Sample acquisition	Data collection	Data processing	Clinical application
Raman spectroscopy	• Tissue • Body fluids • Cell	• Confocal Raman microscope • Raman enhancement instrument	• Multivariate statistical methods • Artificial intelligence • Peak comparison	• Tissue diagnosis of normal and cancerous • Body fluid diagnosis of normal and cancerous • Cell detection for cancer screening
SERS	• Body fluids • Tumor markers • Biomolecules related to tumor • Cell • Tissue • SERS substrate (Addition)	• Confocal Raman microscope • Handheld/ portable Raman spectrometers	• Multivariate statistical methods • Artificial intelligence • Peak comparison	• Detection and analysis of tumor biomarkers • Detection of biomolecules related to tumor growth and dissemination
Raman imaging	• Tissue • Cell • Tumor markers	• Raman enhancement instrument • Confocal Raman microscope • Line scan Raman instrument	• Artificial intelligence • Multivariate statistical methods • Cohen's kappa • Peak comparison	• Tissue diagnosis of normal and cancerous, normal and cancerous subtypes • Cell biochemical and structural feature analysis • Tumor biomarker diagnosis

SERS Surface-enhanced Raman spectroscopy

signal of the detecting substance. However, the added SERS substrate would affect the natural characteristics of samples, which could not really achieve nondestructive testing, compared with the other two methods. Therefore, SERS is used for trace sample detection, such as tumor markers. At the same time, biocompatible SERS substrate should be developed to achieve better diagnostic effect.

For data collection, confocal Raman instrument is mostly applied if only spectral information is collected. However, due to the weak spontaneous Raman intensity of the sample, SERS technology can be used to increase the signal. In this case, confocal Raman instrument can also be used for collection. However, in order to avoid the influence of SERS substrate on the sample's own signal, some other Raman enhancement techniques, such as SRS, could be adopted to improve the signal. For Raman imaging of samples, SRS technology is often used to enhance the signal to achieve higher resolution imaging due to the weak Raman signal of samples themselves. However, the implementation of these technologies requires more expensive and larger footprint equipment. Therefore, it is supposed to design a cheaper Raman equipment and miniaturize the equipment to finally achieve efficient signal acquisition of samples.

For data processing, the data collected based on Raman spectroscopy and SERS are basically one-dimensional spectral data, mainly including peak intensity information and peak position information, while those based on Raman imaging are usually two-dimensional picture information, including both peak intensity information and peak position information, as well as the information of the sample itself, such as morphology. Therefore, different methods are applied to process the collected data. The former two methods mainly use peak intensity contrast or multivariate statistical methods, where these methods are more accurate when dealing with small sample data, however, there is a bottleneck when dealing with large sample data. At this time, artificial intelligence can be used for analysis, especially for sample classification. The one-dimensional spectral data can be directly input into the artificial intelligence model, or the one-dimensional spectral data can be converted to the two-dimensional Raman encoding figure before the training and validation of the artificial intelligence model. Relatively, artificial intelligence is a better choice when processing Raman images because Raman imaging contains more information. It can not only process a large amount of data analysis, but also be more suitable for processing two-dimensional images. Meanwhile, some new artificial intelligence models, such as convolutional neural network and residual network, can better analyze and classify samples.

For clinical application, Raman spectroscopy can be easily obtained by confocal Raman instruments. Therefore, due to the easy availability of data, Raman spectroscopy is more suitable for the diagnosis of easily available samples, such as normal and cancerous diagnosis of body fluids. In addition, the difference of Raman spectra of different samples mainly lies in the difference of Raman peaks and positions, which are relatively not obvious, so the diagnosis of Raman spectra is more suitable for simple diagnostic applications, such as tissue diagnosis of normal and cancerous and cell detection for cancer screening. However, due to the weak spontaneous Raman intensity of the sample, it usually takes a long integration time to obtain the spectrum with acceptable signal noise ratio. SERS is a very excellent Raman enhancement technology and can realize highly precise target detection. Therefore, SERS is very suitable for the detection of low

concentration biological molecules, such as tumor biomarkers, and biomolecules related to tumor growth and dissemination. Raman spectroscopy and SERS methods mainly utilize the spectra to diagnosis, which contains less biological information. Raman imaging can not only obtain the spectral information, as well as the three-dimensional spatial imaging information, but also obtain the geometric shape, molecular structure, and dynamic characteristics of the research object. Hence, Raman imaging is more suitable for imaging tissue samples to analyze the benign and malignant tissues and subtypes. Further, Raman imaging can also be used to analyze cellular biochemical and structural characteristics, and tumor biomarker diagnosis. The appropriate method should be selected based on the samples and the equipment.

In a word, the diagnosis methods of tumor are constantly developing. How to detect, diagnose and treat tumors as early as possible is particularly crucial for human life and health. For early tumor diagnosis, some tumor markers can play a reference significance. However, how to ensure the accuracy of these tumor markers is the most important thing to realize early tumor diagnosis. For these tumor markers with small content, the SERS method could enhance their signal, thus achieving accurate diagnosis of early tumors. However, when the tumor develops to the stage of excision, imaging is usually only used as an auxiliary means, because it can only identify the initial shape of the tumor and cannot accurately distinguish the benign and malignant tumors. Therefore, endoscope/probe-based Raman diagnostic method can be applied to achieve tumor diagnosis and guided resection. For histopathology, the gold standard of tumor diagnosis, necessitates multiple processing steps, and interpretation by a pathologist, which is time, resource, and labor intensive. Here, the diagnostic method based on Raman imaging can streamlined the tumor diagnosis, creating a complementary pathway for tissue diagnosis that is independent of a traditional pathology. In particular, the near real-time SRH+AI diagnostic method can deliver rapid intraoperative pathological diagnosis, greatly minish the waiting time for pathological diagnosis results with compressing the operation time and reducing the damage to patients.

With the development of computer science, applying AI algorithm to classify and diagnose Raman spectra from tumors is the key to greatly improve the accuracy of tumor diagnosis. Two main challenges of using AI to realize tumor diagnosis and cancer detection remain. The first challenge is data set acquisition. At present, the data set acquisition method is still manual. However, in the actual process of data acquisition, the specific parameters or processes used in sample preparation, instrument operation, data labeling and other steps vary from person to person, which will cause certain differences in the data collected by different groups of research, so that the model established according to the data cannot be universal. Secondly, most data sets are obtained from single-center sources. Although single-center studies are favored by researchers due to fewer restrictions on conditions and convenient cooperation, multi-center studies are more suitable for the application of AI for diagnosis. On the one hand, multi-center studies can obtain more data; on the other hand, multi-center studies can achieve data consistency and comparability. Thereby gaining experience in establishing standardized processes. The second challenge is the transparency and interpretability of the models. At present, AI research is largely results-oriented, but the black-box nature of the training process makes the models much less interpretable, and thus less acceptable to

clinicians when it comes to clinical applications. Therefore, it is necessary to establish a transparent model to realize the interpretability of its process, so as to dispel the doubt of clinicians and build trust in it. Still, the research on the interpretability and visualization of deep learning model is still in the initial stage, and more researchers are expected to explore it.

Future clinical applications can be explored and studied from the following two aspects. The first is to do as many multi-center studies as possible. Since most current studies are single-center, there is poor data consistency among various studies, and in-depth comparison cannot be made. Therefore, conducting multi-center studies can not only improve the consistency and comparability of data, but also establish normative procedures and eventually form consensus standards, laying a foundation for actual clinical application. The second aspect is the equipment miniaturization. The Raman equipment used by most of research covers a large area and is fixed in one location. However, stationary and large footprint devices are a major obstacle to clinical application and, in particular, to near-real-time intraoperative diagnosis. Therefore, it is necessary to explore and study the miniaturization of Raman equipment, which can be explored from two directions: handheld probe + Raman spectrometer or miniaturized portable Raman spectrometer.

Anyway, the tumor diagnosis method based on Raman spectroscopy has a broad application prospect. Especially the artificial intelligence fusion with Raman spectroscopy can provide an effective supplement to the existing tumor diagnosis methods, and even replace the existing diagnostic methods in the near future.

Abbreviations

WHO	World health organization
SNR	Signal noise ratio
SERS	Surface-enhanced Raman spectroscopy
SRH	Stimulated Raman histology
1D	One-dimensional
2D	Two-dimensional
AI	Artificial intelligence
PCA	Principal components analysis
LDA	Linear discriminate analysis
QDA	Quadratic discriminant analysis
PLS	Partial least squares
FFPE	Formalin fixation paraffin-embedding
DA	Discriminate analysis
EVs	Extracellular vesicles
SPARTA	Single particle automated Raman trapping analysis
NIR	Near infrared
KCA	K-means cluster analysis
GA	Genetic algorithm
ML	Machine learning
SVM	Support-vector machines
RF	Random forest
KNN	K-nearest neighbors
MR	Marginal relevance
CNN	Convolutional neural network
RNN	Recursive neural network
SSTFT	Spectral short-time Fourier transform
SRP	Spectral recurrence plot
SGAF	Spectral Gramian angular field
SMTF	Spectral Markov transition field
BT	Boosted tree
3D	Three-dimensional
CEA	Carcinoembryonic antigen
EpCAM	Epithelial cell adhesion molecule

EGFR	Epidermal growth factor receptors
MMPs	Matrix metalloproteinases
miRNAs	Micro RNAs
NPs	Nanoparticles
LOD	Limit of detection
LOQ	Limit of quantification
CTCs	Circulating tumor cells
VEGF	Vascular endothelial growth factor
LC	Liver cancer
T	Tumor
NSCLC	Non-small-cell lung cancer
SCLC	Small cell lung cancer
CSCs	Cancer stem cells
CT	Classification tree
Au NRs	Gold nanorods
Au NSs	Gold nanostars
LR	Logistic regression
NCs	Nanocubes
PSA	Prostate specific antigen
Ag NPs	Silver nanoparticles
Ag NRs	Silver nanorods
AFP	*a*-Fetoprotein
BCC	Basal cell carcinoma
FTIR	Fourier transform infrared
RS	Raman spectroscopic
LDs	Lipid droplets
ARMI	Autofluorescence-Raman mapping integration
SRS	Stimulated Raman scattering
H&E	Hematoxylin and eosin
IHC	Immunohistochemistry
RCI	Raman chemical imaging
CRM	Confocal Raman microscope
HAp	Hydroxyapatite
LSRM	Line scan Raman microspectroscopy
NHDF	Normal human dermal fibroblasts
PCs	Principal components
CWT	Continuous wavelet transform

Availability of data and materials
Not applicable.

Declarations

Competing interests
The authors declare that they have no competing interests.

References
1. Sung H, Ferlay J, Siegel RL, Laversanne M, Soerjomataram I, Jemal A, Bray F. Global cancer statistics 2020: Globocan estimates of incidence and mortality worldwide for 36 cancers in 185 countries. CA-Cancer J Clin. 2021;71(3):209–49.
2. Inamura K, Ishikawa Y. MicroRNA in lung cancer: Novel biomarkers and potential tools for treatment. J Clin Med. 2016;5:36.
3. Luo X, Liu J, Wang H, Lu H. Metabolomics identified new biomarkers for the precise diagnosis of pancreatic cancer and associated tissue metastasis. Pharmacol Res. 2020;156: 104805.
4. Huang Q, Ouyang X. Predictive biochemical-markers for the development of brain metastases from lung cancer: Clinical evidence and future directions. Cancer Epidemiol. 2013;37(5):703–7.

5. Vansteenkiste J, Fischer BM, Dooms C, Mortensen J. Positron-emission tomography in prognostic and therapeutic assessment of lung cancer: Systematic review. Lancet Oncol. 2004;5(9):531–40.

6. Lian C, Ruan S, Denœux T, Jardin F, Vera P. Selecting radiomic features from FDG-PET images for cancer treatment outcome prediction. Med Image Anal. 2016;32:257–68.

7. Reboucas PP, Cortez PC, Barros ACD, Albuquerque VHC, Tavares JMRS. Novel and powerful 3D adaptive crisp active contour method applied in the segmentation of CT lung images. Med Image Anal. 2017;35:503–16.

8. Gal AA. In search of the origins of modern surgical pathology. Adv Anat Pathol. 2001;8(1):1–13.

9. Gutmann EJ. Pathologists and patients: Can we talk? Mod Pathol. 2003;16(5):515–8.

10. Lechago J. The frozen section - Pathology in the trenches. Arch Pathol Lab Med. 2005;129(12):1529–31.

11. Gal AA, Cagle PT. The 100-year anniversary of the description of the frozen section procedure. JAMA-J Am Med Assoc. 2005;294(24):3135–7.

12. Qi YF, Liu YH, Liu DM. Research progress on application of Raman spectroscopy in tumor diagnosis. Laser Opto-electron Prog. 2020;57(22): 220001.

13. Movasaghi Z, Rehman S, Rehman IU. Raman spectroscopy of biological tissues. Appl Spectrosc Rev. 2007;42(5):493–541.

14. Hollon T, Orringer DA. Label-free brain tumor imaging using Raman-based methods. J Neuro-Oncol. 2021;151(3):393–402.

15. Butler HJ, Ashton L, Bird B, Cinque G, Curtis K, Dorney J, Esmonde-White K, Fullwood NJ, Gardner B, Martin-Hirsch PL, Walsh MJ, McAinsh MR, Stone N, Martin FL. Using Raman spectroscopy to characterize biological materials. Nat Protoc. 2016;11(4):664–87.

16. Ralbovsky NM, Lednev IK. Towards development of a novel universal medical diagnostic method: Raman spectroscopy and machine learning. Chem Soc Rev. 2020;49(20):7428–53.

17. Chase B. A new-generation of Raman instrumentation. Appl Spectrosc. 1994;48(7):A14–9.

18. Zhou J, Pan W, Qi W, Cao X, Cheng Z, Feng Y. Ultrafast Raman fiber laser: A review and prospect. PhotoniX. 2022;3:18.

19. Ye J, Ma X, Zhang Y, Xu J, Zhang H, Yao T, Leng J, Zhou P. From spectral broadening to recompression: Dynamics of incoherent optical waves propagating in the fiber. PhotoniX. 2021;2:15.

20. Lin T, Song Y-L, Kuang P, Chen S, Mao Z, Zeng T-T. Nanostructure-based surface-enhanced Raman scattering for diagnosis of cancer. Nanomedicine. 2021;16(26):2389–406.

21. Li L, Yang J, Wei J, Jiang C, Liu Z, Yang B, Zhao B, Song W. SERS monitoring of photoinduced-enhanced oxidative stress amplifier on Au@carbon dots for tumor catalytic therapy. Light Sci Appl. 2022;11(1):286.

22. Wang H-L, You E-M, Panneerselvam R, Ding S-Y, Tian Z-Q. Advances of surface-enhanced Raman and IR spectroscopies: from nano/microstructures to macro-optical design. Light Sci Appl. 2021;10(1):161.

23. Ding SY, You EM, Tian ZQ, Moskovits M. Electromagnetic theories of surface-enhanced Raman spectroscopy. Chem Soc Rev. 2017;46(13):4042–76.

24. Yang W, Knorr F, Latka I, Vogt M, Hofmann GO, Popp J, Schie IW. Real-time molecular imaging of near-surface tissue using Raman spectroscopy. Light Sci Appl. 2022;11(1):90.

25. Ilchenko O, Pilhun Y, Kutsyk A. Towards Raman imaging of centimeter scale tissue areas for real-time opto-molecular visualization of tissue boundaries for clinical applications. Light Sci Appl. 2022;11(1):143.

26. Ao J, Feng Y, Wu S, Wang T, Ling J, Zhang L, Ji M. Rapid, 3D chemical profiling of individual atmospheric aerosols with stimulated Raman scattering microscopy. Small Methods. 2019;4(2):1900600.

27. Ao J, Fang X, Miao X, Ling J, Kang H, Park S, Wu C, Ji M. Switchable stimulated Raman scattering microscopy with photochromic vibrational probes. Nat Commun. 2021;12(1):3089.

28. Kong CH, Pilger C, Hachmeister H, Wei XM, Cheung TH, Lai CSW, Lee NP, Tsia KK, Wong KKY, Huser T. High-contrast, fast chemical imaging by coherent Raman scattering using a self-synchronized two-colour fibre laser. Light Sci Appl. 2020;9:25.

29. Li J, Zhang MJ. Physics and applications of Raman distributed optical fiber sensing. Light Sci Appl. 2022;11:128.

30. Wang T, Jiang J, Liu K, Wang S, Niu P, Liu Y, Liu T. Flexible minimally invasive coherent anti-Stokes Raman spectroscopy (CARS) measurement method with tapered optical fiber probe for single-cell application. PhotoniX. 2022;3:11.

31. Hollon TC, Pandian B, Adapa AR, Urias E, Save AV, Khalsa SSS, Eichberg DG, D'Amico RS, Farooq ZU, Lewis S, Petridis PD, Marie T, Shah AH, Garton HJL, Maher CO, Heth JA, McKean EL, Sullivan SE, Hervey-Jumper SL, Patil PG, Thompson BG, Sagher O, McKhann GM, Komotar RJ 2nd, Ivan ME, Snuderl M, Otten ML, Johnson TD, Sisti MB, Bruce JN, Muraszko KM, Trautman J, Freudiger CW, Canoll P, Lee H, Camelo-Piragua S, Orringer DA. Near real-time intraoperative brain tumor diagnosis using stimulated Raman histology and deep neural networks. Nat Med. 2020;26(1):52–8.

32. He H, Yan S, Lyu D, Xu M, Ye R, Zheng P, Lu X, Wang L, Ren B. Deep learning for biospectroscopy and biospectral imaging: State-of-the-art and perspectives. Anal Chem. 2021;93(8):3653–65.

33. Aguiar RP, Falcao ET, Pasqualucci CA, Silveira L Jr. Use of Raman spectroscopy to evaluate the biochemical composition of normal and tumoral human brain tissues for diagnosis. Lasers Med Sci. 2022;37(1):121–33.

34. Kaushik R, Rani C, Neeshu K, Tanwar M, Pathak DK, Chaudhary A, Siraj F, Jha HC, Kumar R. Brain tumour detection and grading using Raman scattering: Analogy from semiconductors for solving biological problem. Adv Mater Process Technol. 2020;8(1):703–14.

35. Kopec M, Blaszczyk M, Radek M, Abramczyk H. Raman imaging and statistical methods for analysis various type of human brain tumors and breast cancers. Spectroc Acta Pt A-Molec Biomolec Spectr. 2021;262: 120091.

36. Livermore LJ, Isabelle M, Bell IM, Edgar O, Voets NL, Stacey R, Ansorge O, Vallance C, Plaha P. Raman spectroscopy to differentiate between fresh tissue samples of glioma and normal brain: A comparison with 5-ALA-induced fluorescence-guided surgery. J Neurosurg. 2021;132(2):469–79.

37. Depciuch J, Tolpa B, Witek P, Szmuc K, Kaznowska E, Osuchowski M, Krol P, Cebulski J. Raman and FTIR spectroscopy in determining the chemical changes in healthy brain tissues and glioblastoma tumor tissues. Spectroc Acta Pt A-Molec Biomolec Spectr. 2020;225: 117526.

38. Iturrioz-Rodriguez N, De Pasquale D, Fiaschi P, Ciofani G. Discrimination of glioma patient-derived cells from healthy astrocytes by exploiting Raman spectroscopy. Spectroc Acta Pt A-Molec Biomolec Spectr. 2022;269: 120773.

39. Lilo T, Morais CLM, Ashton KM, Davis C, Dawson TP, Martin FL, Alder J, Roberts G, Ray A, Gurusinghe N. Raman hyperspectral imaging coupled to three-dimensional discriminant analysis: Classification of meningiomas brain tumour grades. Spectroc Acta Pt A-Molec Biomolec Spectr. 2022;273: 121018.

40. Zhang C, Han Y, Sun B, Zhang W, Liu S, Liu J, Lv H, Zhang G, Kang X. Label-free serum detection based on Raman spectroscopy for the diagnosis and classification of glioma. J Raman Spectrosc. 2020;51(10):1977–85.

41. Ning T, Li H, Chen Y, Zhang B, Zhang F, Wang S. Raman spectroscopy based pathological analysis and discrimination of formalin fixed paraffin embedded breast cancer tissue. Vib Spectrosc. 2021;115: 103260.

42. Li H, Ning T, Yu F, Chen Y, Zhang B, Wang S. Raman microspectroscopic investigation and classification of breast cancer pathological characteristics. Molecules. 2021;26(4):921.

43. Wang S, Li H, Ren Y, Yu F, Song D, Zhu L, Yu S, Jiang S, Zeng H. Studying the pathological and biochemical features in breast cancer progression by confocal Raman microspectral imaging of excised tissue samples. J Photochem Photobiol B-Biol. 2021;222: 112280.

44. Wen X, Ou Y-C, Bogatcheva G, Thomas G, Mahadevan-Jansen A, Singh B, Lin EC, Bardhan R. Probing metabolic alterations in breast cancer in response to molecular inhibitors with Raman spectroscopy and validated with mass spectrometry. Chem Sci. 2020;11(36):9863–74.

45. Maitra I, Morais CLM, Lima KMG, Ashton KM, Date RS, Martin FL. Raman spectral discrimination in human liquid biopsies of oesophageal transformation to adenocarcinoma. J Biophotonics. 2020;13(3): e201960132.

46. Liang H, Cheng X, Dong S, Wang H, Liu E, Ru Y, Li Y, Kong X, Gao Y. Rapid and non-invasive discrimination of acute leukemia bone marrow supernatants by Raman spectroscopy and multivariate statistical analysis. J Pharm Biomed Anal. 2022;210: 114560.

47. Kirchberger-Tolstik T, Ryabchykov O, Bocklitz T, Dirsch O, Settmacher U, Popp J, Stallmach A. Nondestructive molecular imaging by Raman spectroscopy vs. marker detection by MALDI IMS for an early diagnosis of HCC. Analyst. 2021;146(4):1239–52.

48. Song D, Chen T, Wang S, Chen S, Li H, Yu F, Zhang J, Zhang Z. Study on the biochemical mechanisms of the micro-wave ablation treatment of lung cancer by ex vivo confocal Raman microspectral imaging. Analyst. 2020;145(2):626–35.

49. Yang X, Wu Z, Ou Q, Qian K, Jiang L, Yang W, Shi Y, Liu G. Diagnosis of lung cancer by FTIR spectroscopy combined with Raman spectroscopy based on data fusion and wavelet transform. Front Chem. 2022;10: 810837.

50. Song D, Yu F, Chen S, Chen Y, He Q, Zhang Z, Zhang J, Wang S. Raman spectroscopy combined with multivariate analysis to study the biochemical mechanism of lung cancer microwave ablation. Biomed Opt Express. 2020;11(2):1061–72.

51. Sharma M, Jeng M-J, Young C-K, Huang S-F, Chang L-B. Developing an algorithm for discriminating oral cancerous and normal tissues using Raman spectroscopy. J Pers Med. 2021;11(11):1165.

52. Falamas A, Faur CI, Baciut M, Rotaru H, Chirila M, Cinta Pinzaru S, Hedesiu M. Raman spectroscopic characterization of saliva for the discrimination of oral squamous cell carcinoma. Anal Lett. 2021;54(1–2):57–69.

53. Fan L, Wang H, Wu X, Wang S, Han Y, Wang J. Raman spectroscopic study of benign and malignant ovarian tissues. Laser Phys. 2022;32(3): 035601.

54. Paluszkiewicz C, Roman M, Piergies N, Pieta E, Wozniak M, Guidi MC, Miskiewicz-Orczyk K, Markow M, Scierski W, Misiolek M, Drozdzowska B, Kwiatek WM. Tracking of the biochemical changes upon pleomorphic adenoma progression using vibrational microspectroscopy. Sci Rep. 2021;11(1):18010.

55. Kirkby CJ, de Pablo JG, Tinkler-Hundal E, Wood HM, Evans SD, West NP. Developing a Raman spectroscopy-based tool to stratify patient response to pre-operative radiotherapy in rectal cancer. Analyst. 2021;146(2):581–9.

56. Ruiz JJ, Marro M, Galvan I, Bernabeu-Wittel J, Conejo-Mir J, Zulueta-Dorado T, Guisado-Gil AB, Loza-Alvarez P. Novel non-invasive quantification and imaging of eumelanin and DHICA subunit in skin lesions by Raman spectroscopy and MCR algorithm: Improving dysplastic nevi diagnosis. Cancers. 2022;14(4):1056.

57. Silveira L Jr, Pasqualucci CA, Bodanese B, Tavares Pacheco MT, Zangaro RA. Normal-subtracted preprocessing of Raman spectra aiming to discriminate skin actinic keratosis and neoplasias from benign lesions and normal skin tissues. Lasers Med Sci. 2020;35(5):1141–51.

58. Zhang W, Karagiannidis I, Van Vliet ED, Yao RX, Beswick EJ, Zhou AH. Granulocyte colony-stimulating factor promotes an aggressive phenotype of colon and breast cancer cells with biochemical changes investigated by single-cell Raman microspectroscopy and machine learning analysis. Analyst. 2021;146(20):6124–31.

59. Beton K, Brozek-Pluska B. Vitamin C-protective role in oxidative stress conditions induced in human normal colon cells by label-free Raman spectroscopy and imaging. Int J Mol Sci. 2021;22(13):6928.

60. Iwasaki Y, Kawagishi M, Takase H, Ohno-Matsui K. Discrimination of dissociated lymphoma cells from leukocytes by Raman spectroscopy. Sci Rep. 2020;10(1):15778.

61. Sciortino T, Secoli R, d'Amico E, Moccia S, Conti Nibali M, Gay L, Rossi M, Pecco N, Castellano A, De Momi E, Fernandes B, Riva M, Bello L. Raman spectroscopy and machine learning for IDH genotyping of unprocessed glioma biopsies. Cancers. 2021;13(16):4196.

62. Riva M, Sciortino T, Secoli R, D'Amico E, Moccia S, Fernandes B, Conti Nibali M, Gay L, Rossi M, De Momi E, Bello L. Glioma biopsies classification using Raman spectroscopy and machine learning models on fresh tissue samples. Cancers. 2021;13(5):1073.

63. Zhang L, Li C, Peng D, Yi X, He S, Liu F, Zheng X, Huang WE, Zhao L, Huang X. Raman spectroscopy and machine learning for the classification of breast cancers. Spectroc Acta Pt A-Molec Biomolec Spectr. 2022;264: 120300.

64. Zhang H, Chen C, Ma C, Chen C, Zhu Z, Yang B, Chen F, Jia D, Li Y, Lv X. Feature fusion combined with Raman spectroscopy for early diagnosis of cervical cancer. IEEE Photonics J. 2021;13(3):3900311.

65. He C, Zhu S, Wu X, Zhou J, Chen Y, Qian X, Ye J. Accurate tumor subtype detection with Raman spectroscopy via variational autoencoder and machine learning. ACS Omega. 2022;7(12):10458–68.

66. He C, Wu X, Zhou J, Chen Y, Ye J. Raman optical identification of renal cell carcinoma via machine learning. Spectroc Acta Pt A-Molec Biomolec Spectr. 2021;252: 119520.

67. Jelke F, Mirizzi G, Borgmann FK, Husch A, Slimani R, Klamminger GG, Klein K, Mombaerts L, Gerardy J-J, Mittelbronn M, Hertel F. Intraoperative discrimination of native meningioma and dura mater by Raman spectroscopy. Sci Rep. 2021;11(1):23583.

68. Lau CPY, Ma W, Law KY, Lacambra MD, Wong KC, Lee CW, Lee OK, Dou Q, Kumta SM. Development of deep learning algorithms to discriminate giant cell tumors of bone from adjacent normal tissues by confocal Raman spectroscopy. Analyst. 2022;147(7):1425–39.

69. Huang X, Song D, Li J, Qin J, Wang D, Li J, Wang H, Wang S. Validating multivariate classification algorithms in Raman spectroscopy-based osteosarcoma cellular analysis. Anal Lett. 2021;55(7):1052–67.

70. Ma DY, Shang LW, Tang JL, Bao YL, Fu JJ, Yin JH. Classifying breast cancer tissue by Raman spectroscopy with one-dimensional convolutional neural network. Spectroc Acta Pt A-Molec Biomolec Spectr. 2021;256: 119732.

71. Conforti PM, D'Acunto M, Russo P. Deep learning for chondrogenic tumor classification through wavelet transform of Raman spectra. Sensors. 2022;22:7492.

72. Wu X, Li S, Xu Q, Yan X, Fu Q, Fu X, Fang X, Zhang Y. Rapid and accurate identification of colon cancer by Raman spectroscopy coupled with convolutional neural networks. Jpn J Appl Phys. 2021;60(6): 067001.

73. Li Z, Li Z, Chen Q, Zhang J, Dunham ME, McWhorter AJ, Feng J-M, Li Y, Yao S, Xu J. Machine-learning-assisted spontaneous Raman spectroscopy classification and feature extraction for the diagnosis of human laryngeal cancer. Comput Biol Med. 2022;146: 105617.

74. Qi Y, Yang L, Liu B, Liu L, Liu Y, Zheng Q, Liu D, Luo J. Accurate diagnosis of lung tissues for 2D Raman spectrogram by deep learning based on short-time Fourier transform. Anal Chim Acta. 2021;1179: 338821.

75. Qi Y, Yang L, Liu B, Liu L, Liu Y, Zheng Q, Liu D, Luo J. Highly accurate diagnosis of lung adenocarcinoma and squamous cell carcinoma tissues by deep learning. Spectroc Acta Pt A-Molec Biomolec Spectr. 2022;265: 120400.

76. Qi Y, Zhang G, Yang L, Liu B, Zeng H, Xue Q, Liu D, Zheng Q, Liu Y. High-precision intelligent cancer diagnosis method: 2D Raman figures combined with deep learning. Anal Chem. 2022;94(17):6491–501.

77. Xia J, Zhu L, Yu M, Zhang T, Zhu Z, Lou X, Sun G, Dong M. Analysis and classification of oral tongue squamous cell carcinoma based on Raman spectroscopy and convolutional neural networks. J Mod Opt. 2020;67(6):481–9.

78. Yan H, Yu MX, Xia JB, Zhu LQ, Zhang T, Zhu ZH, Sun GK. Diverse region-based CNN for tongue squamous cell carcinoma classification with Raman spectroscopy. IEEE Access. 2020;8:127313–28.

79. Li Z, Li Z, Chen Q, Ramos A, Zhang J, Boudreaux JP, Thiagarajan R, Bren-Mattison Y, Dunham ME, McWhorter AJ, Li X, Feng J-M, Li Y, Yao S, Xu J. Detection of pancreatic cancer by convolutional-neural-network-assisted spontaneous Raman spectroscopy with critical feature visualization. Neural Netw. 2021;144:455–64.

80. Bratchenko IA, Bratchenko LA, Khristoforova YA, Moryatov AA, Kozlo SV, Zakharo VP. Classification of skin cancer using convolutional neural networks analysis of Raman spectra. Comput Meth Programs Biomed. 2022;219:106755.

81. O'Dwyer K, Domijan K, Dignam A, Butler M, Hennelly BM. Automated Raman micro-spectroscopy of epithelial cell nuclei for high-throughput classification. Cancers. 2021;13(19):4767.

82. Iwasaki K, Araki A, Krishna CM, Maruyama R, Yamamoto T, Noothalapati H. Identification of molecular basis for objective discrimination of breast cancer cells (MCF-7) from normal human mammary epithelial cells by Raman microspectroscopy and multivariate curve resolution analysis. Int J Mol Sci. 2021;22(2):800.

83. Santos IP, Martins CB, de Carvalho LAEB, Marques MPM, de Carvalho ALMB. Who's who? Discrimination of human breast cancer cell lines by Raman and FTIR microspectroscopy. Cancers. 2022;14(2):452.

84. Bukva M, Dobra G, Gomez-Perez J, Koos K, Harmati M, Gyukity-Sebestyen E, Biro T, Jenei A, Kormondi S, Horvath P, Konya Z, Klekner A, Buzas K. Raman spectral signatures of serum-derived extracellular vesicle-enriched isolates may support the diagnosis of CNS tumors. Cancers. 2021;13(6):1407.

85. Mandrell CT, Holland TE, Wheeler JE, Esmaeili SMA, Amar K, Chowdhury F, Sivakumar P. Machine learning approach to Raman spectrum analysis of MIA PaCa-2 pancreatic cancer tumor repopulating cells for classification and feature analysis. Life. 2020;10(9):181.

86. Ma MR, Tian XC, Chen FF, Ma XJ, Guo WJ, Lv XY. The application of feature engineering in establishing a rapid and robust model for identifying patients with glioma. Lasers Med Sci. 2022;37(2):1007–15.

87. Ito H, Uragami N, Miyazaki T, Yang W, Issha K, Matsuo K, Kimura S, Arai Y, Tokunaga H, Okada S, Kawamura M, Yokoyama N, Kushima M, Inoue H, Fukagai T, Kamijo Y. Highly accurate colorectal cancer prediction model based on Raman spectroscopy using patient serum. World J Gastrointest Oncol. 2020;12(11):1311–24.

88. Giamougiannis P, Silva RVO, Freitas DLD, Lima KMG, Anagnostopoulos A, Angelopoulos G, Naik R, Wood NJ, Martin-Hirsch PL, Martin FL. Raman spectroscopy of blood and urine liquid biopsies for ovarian cancer diagnosis: Identification of chemotherapy effects. J Biophotonics. 2021;14(11): e202100195.

89. Yan Z, Ma C, Mo J, Han W, Lv X, Chen C, Chen C, Nie X. Rapid identification of benign and malignant pancreatic tumors using serum Raman spectroscopy combined with classification algorithms. Optik. 2020;208: 164473.

90. Tian X, Chen C, Chen C, Yan Z, Wu W, Chen F, Chen J, Lv X. Application of Raman spectroscopy technology based on deep learning algorithm in the rapid diagnosis of glioma. J Raman Spectrosc. 2022;53(4):735–45.

91. Chen C, Wu W, Chen C, Chen F, Dong X, Ma M, Yan Z, Lv X, Ma Y, Zhu M. Rapid diagnosis of lung cancer and glioma based on serum Raman spectroscopy combined with deep learning. J Raman Spectrosc. 2021;52(11):1798–809.

92. Penders J, Nagelkerke A, Cunnane EM, Pedersen SV, Pence IJ, Coombes RC, Stevens MM. Single particle automated Raman trapping analysis of breast cancer cell-derived extracellular vesicles as cancer biomarkers. ACS Nano. 2021;15(11):18192–205.

93. Atkins CG, Buckley K, Blades MW, Turner RFB. Raman spectroscopy of blood and blood components. Appl Spectrosc. 2017;71(5):767–93.

94. Chen GY, Qian SE. Denoising of hyperspectral imagery using principal component analysis and wavelet shrinkage. IEEE Trans Geosci Remote Sensing. 2011;49(3):973–80.

95. Trevisan J, Angelov PP, Carmichael PL, Scott AD, Martin FL. Extracting biological information with computational analysis of Fourier-transform infrared (FTIR) biospectroscopy datasets: Current practices to future perspectives. Analyst. 2012;137:3202–15.

96. Jarvis RM, Goodacre R. Genetic algorithm optimization for pre-processing and variable selection of spectroscopic data. Bioinformatics. 2005;21(7):860–8.

97. Martin FL, Kelly JG, Llabjani V, Martin-Hirsch PL, Patel II, Trevisan J, Fullwood NJ, Walsh MJ. Distinguishing cell types or populations based on the computational analysis of their infrared spectra. Nat Protoc. 2010;5(11):1748–60.

98. Tang M, Xia L, Wei D, Yan S, Du C, Cui H-L. Distinguishing different cancerous human cells by Raman spectroscopy based on discriminant analysis methods. Appl Sci. 2017;7:900.

99. Jain AK, Duin RPW, Mao JC. Statistical pattern recognition: A review. IEEE Trans Pattern Anal Mach Intell. 2000;22(1):4–37.

100. He Q, Yang W, Luo W, Wilhelm S, Weng B. Label-free differentiation of cancer and non-cancer cells based on machine-learning-algorithm-assisted fast Raman imaging. Biosensors. 2022;12(4):250.

101. Wen J, Tang T, Kanwal S, Lu Y, Tao C, Zheng L, Zhang D, Gu Z. Detection and classification of multi-type cells by using confocal Raman spectroscopy. Front Chem. 2021;9: 641670.

102. Cortes C, Vapnik V. Support-vector networks. Mach Learn. 1995;20(3):273–97.

103. Noori R, Abdoli MA, Ghasrodashti AA, Ghazizade MJ. Prediction of municipal solid waste generation with combination of support vector machine and principal component analysis: A case study of Mashhad. Environ Prog Sustain Energy. 2009;28(2):249–58.

104. You HH, Ma ZY, Tang YJ, Wang YL, Yan JH, Ni MJ, Cen KF, Huang QX. Comparison of ANN (MLP), ANFIS, SVM, and RF models for the online classification of heating value of burning municipal solid waste in circulating fluidized bed incinerators. Waste Manage. 2017;68:186–97.

105. Svetnik V, Liaw A, Tong C, Culberson JC, Sheridan RP, Feuston BP. Random forest: A classification and regression tool for compound classification and QSAR modeling. J Chem Inf Comput Sci. 2003;43(6):1947–58.

106. Dhanabal S, Chandramathi SA. A review of various k-nearest neighbor query processing techniques. Int J Comput Appl. 2011;31(7):14–22.

107. Krizhevsky A, Sutskever I, Hinton GE. Imagenet classification with deep convolutional neural networks. Commun ACM. 2017;60(6):84–90.

108. He K M, Zhang X Y, Ren S Q, Sun J. Deep residual learning for image recognition. In: Proceedings of the 2016 IEEE Conference on Computer Vision and Pattern Recognition. Las Vegas: IEEE; 2016. p. 770-8.

109. Szegedy C, Liu W, Jia Y Q, Sermanet P, Reed S, Anguelov D, Erhan D, Vanhoucke V, Rabinovich A. Going deeper with convolutions. In: Proceedings of the 2015 IEEE Conference on Computer Vision and Pattern Recognition. Boston, MA, USA: IEEE, 2015; 1-9.

110. Zia T, Zahid U. Long short-term memory recurrent neural network architectures for Urdu acoustic modeling. Int J Speech Technol. 2019;22(1):21–30.

111. Liang X, Zhang P, Ma M, Yang T, Zhao X, Zhang R, Jing M, Song R, Wang L, Fan J. Multiplex ratiometric gold nanoprobes based on surface-enhanced Raman scattering enable accurate molecular detection and imaging of bladder cancer. Nano Res. 2022;15(4):3487–95.

112. Qian H, Wang Y, Ma Z, Qian L, Shao X, Jin D, Cao M, Liu S, Chen H, Pan J, Xue W. Surface-enhanced Raman spectroscopy of pretreated plasma samples predicts disease recurrence in muscle-invasive bladder cancer patients undergoing neoadjuvant chemotherapy and radical cystectomy. Int J Nanomed. 2022;17:1635–46.

113. Hu D, Xu X, Zhao Z, Li C, Tian Y, Liu Q, Shao B, Chen S, Zhao Y, Li L, Bi H, Chen A, Fu C, Cui X, Zeng Y. Detecting urine metabolites of bladder cancer by surface-enhanced Raman spectroscopy. Spectroc Acta Pt A-Molec Biomolec Spectr. 2021;247: 119108.

114. Li J, Wang C, Yao Y, Zhu Y, Yan C, Zhuge Q, Qu L, Han C. Label-free discrimination of glioma brain tumors in different stages by surface enhanced Raman scattering. Talanta. 2020;216: 120983.

115. Kowalska AA, Berus S, Szleszkowski L, Kaminska A, Kmiecik A, Ratajczak-Wielgomas K, Jurek T, Zadka L. Brain tumour homogenates analysed by surface-enhanced Raman spectroscopy: Discrimination among healthy and cancer cells. Spectroc Acta Pt A-Molec Biomolec Spectr. 2020;231: 117769.

116. Kowalska AA, Czaplicka M, Nowicka AB, Nicinski K, Piotrowska A, Kaminska A. Association between grade brain tumors and the interleukin-10 receptor subunit alpha based on surface-enhanced Raman spectroscopy and multivariate analysis. J Raman Spectrosc. 2021;52(11):1788–97.

117. Kim J, Park J, Ki J, Rho HW, Huh Y-M, Kim E, Son HY, Haam S. Simultaneous dual-targeted monitoring of breast cancer circulating miRNA via surface-enhanced Raman spectroscopy. Biosens Bioelectron. 2022;207: 114143.

118. Liu S, Su H-S, Yang Z, Zhang Y. Ag nanorods for label-free surface-enhanced Raman scattering analysis of cancer cells from cell lysates. ACS Appl Nano Mater. 2022;5(1):269–76.

119. Lee W-J, Kim K-J, Hossain MK, Cho H-Y, Choi J-W. DNA-gold nanoparticle conjugates for intracellular miRNA detection using surface-enhanced Raman spectroscopy. BioChip J. 2022;16(1):33–40.

120. Jibin K, Babu RV, Jayasree RS. Graphene-gold nanohybrid-based surface-enhanced Raman scattering platform on a portable easy-to-use centrifugal prototype for liquid biopsy detection of circulating breast cancer cells. ACS Sustain Chem Eng. 2021;9(46):15496–505.

121. Zhao Y, Fang X, Bai M, Zhang J, Yu H, Chen F, Zhao Y. A microfluidic surface-enhanced Raman scattering (SERS) sensor for microRNA in extracellular vesicles with nucleic acid-tyramine cascade amplification. Chin Chem Lett. 2022;33(4):2101–4.

122. Kim S, Kim TG, Lee SH, Kim W, Bang A, Moon SW, Song J, Shin J-H, Yu JS, Choi S. Label-free surface-enhanced Raman spectroscopy biosensor for on-site breast cancer detection using human tears. ACS Appl Mater Inter. 2020;12(7):7897–904.

123. Gao N, Wang Q, Tang J, Yao S, Li H, Yue X, Fu J, Zhong F, Wang T, Wang J. Non-invasive SERS serum detection technology combined with multivariate statistical algorithm for simultaneous screening of cervical cancer and breast cancer. Anal Bioanal Chem. 2021;413(19):4775–84.

124. Keshavarz M, Kassanos P, Tan B, Venkatakrishnan K. Metal-oxide surface-enhanced Raman biosensor template towards point-of-care EGFR detection and cancer diagnostics. Nanoscale Horiz. 2020;5(2):294–307.

125. Wang J, Xie H, Ding C. Designed co-DNA-locker and ratiometric SERS sensing for accurate detection of exosomes based on gold nanorod arrays. ACS Appl Mater Inter. 2021;13(28):32837–44.

126. Xu X, Lin J, Guo Y, Wu X, Xu Y, Zhang D, Zhang X, Yujiao X, Wang J, Yao C, Yao J, Xing J, Cao Y, Li Y, Ren W, Chen T, Ren Y, Wu A. TiO2-based surface-enhanced Raman scattering bio-probe for efficient circulating tumor cell detection on microfilter. Biosens Bioelectron. 2022;210: 114305.

127. Karunakaran V, Saritha VN, Ramya AN, Murali VP, Raghu KG, Sujathan K, Maiti KK. Elucidating Raman image-guided differential recognition of clinically confirmed grades of cervical exfoliated cells by dual biomarker-appended SERS-tag. Anal Chem. 2021;93(32):11140–50.

128. Avram L, Iancu SD, Stefancu A, Moisoiu V, Colnita A, Marconi D, Donca V, Buzdugan E, Craciun R, Leopold N, Crisan N, Coman I, Crisan D. SERS-based liquid biopsy of gastrointestinal tumors using a portable Raman device operating in a clinical environment. J Clin Med. 2020;9(1):212.

129. Gao S, Lin Y, Zheng M, Lin Y, Lin K, Xie S, Yu Y, Lin J. Label-free determination of liver cancer stages using surface-enhanced Raman scattering coupled with preferential adsorption of hydroxyapatite microspheres. Anal Methods. 2021;13(35):3885–93.

130. Er E, Sanchez-Iglesias A, Silvestri A, Arnaiz B, Liz-Marzan LM, Prato M, Criado A. Metal nanoparticles/MoS2 surface-enhanced Raman scattering-based sandwich immunoassay for a-fetoprotein detection. ACS Appl Mater Inter. 2021;13(7):8823–31.

131. Gao R, Zhan C, Wu C, Lu Y, Cao B, Huang J, Wang F, Yu L. Simultaneous single-cell phenotype analysis of hepatocellular carcinoma CTCs using a SERS-aptamer based microfluidic chip. Lab Chip. 2021;21(20):3888–98.

132. He M, Lin J, Akakuru OU, Xu XW, Li YY, Cao Y, Xu YP, Wu AG. Octahedral silver oxide nanoparticles enabling remarkable SERS activity for detecting circulating tumor cells. Sci China-Life Sci. 2022;65(3):561–71.

133. Huang Y, Xie T, Zou K, Gu Y, Yang G, Zhang F, Qu L-L, Yang S. Ultrasensitive SERS detection of exhaled biomarkers of lung cancer using a multifunctional solid phase extraction membrane. Nanoscale. 2021;13(31):13344–52.

134. Fan C, Zhao N, Cui K, Chen G, Chen Y, Wu W, Li Q, Cui Y, Li R, Xiao Z. Ultrasensitive exosome detection by modularized SERS labeling for postoperative recurrence surveillance. ACS Sens. 2021;6(9):3234–41.

135. Huang L, Zhang Z, Li G. DNA strand displacement based surface-enhanced Raman scattering-fluorescence dual-mode nanoprobes for quantification and imaging of vascular endothelial growth factor in living cells. Biosens Bioelectron. 2022;204: 114069.

136. Reza KK, Dey S, Wuethrich A, Wang J, Behren A, Antaw F, Wang Y, Ibn Sina AA, Trau M. In situ single cell proteomics reveals circulating tumor cell heterogeneity during treatment. ACS Nano. 2021;15(7):11231–43.

137. Lin D, Hsieh C-L, Hsu K-C, Liao P-H, Qiu S, Gong T, Yong K-T, Feng S, Kong KV. Geometrically encoded SERS nanobarcodes for the logical detection of nasopharyngeal carcinoma-related progression biomarkers. Nat Commun. 2021;12(1):3430.

138. Han Z, Yi J, Yang Y, Li D, Peng C, Long S, Peng X, Shen Y, Liu B, Qiao L. SERS and MALDI-TOF MS based plasma exosome profiling for rapid detection of osteosarcoma. Analyst. 2021;146(21):6496–505.

139. Sujai PT, Shamjith S, Joseph MM, Maiti KK. Elucidating gold-MnO2 core-shell nanoenvelope for real time SERS-guided photothermal therapy on pancreatic cancer cells. ACS Appl Bio Mater. 2021;4(6):4962–72.

140. Hu J, Shao X, Chi C, Zhu Y, Xin Z, Sha J, Dong B, Pan J, Xue W. Surface-enhanced Raman spectroscopy of serum predicts sensitivity to docetaxel-based chemotherapy in patients with metastatic castration-resistant prostate cancer. J Innov Opt Health Sci. 2021;14(04):2141006.

141. Rajput S, Pink D, Findlay S, Woolner E, Lewis JD, McDermott MT. Application of surface-enhanced Raman spectroscopy to guide therapy for advanced prostate cancer patients. ACS Sens. 2022;7(3):827–38.

142. Turan E, Zengin A, Suludere Z, Kalkan NO, Tamer U. Construction of a sensitive and selective plasmonic biosensor for prostate specific antigen by combining magnetic molecularly-imprinted polymer and surface-enhanced Raman spectroscopy. Talanta. 2022;237: 122926.

143. Czaplicka M, Kowalska AA, Nowicka AB, Kurzydlowski D, Gronkiewicz Z, Machulak A, Kukwa W, Kaminska A. Raman spectroscopy and surface-enhanced Raman spectroscopy (SERS) spectra of salivary glands carcinoma, tumor and healthy tissues and their homogenates analyzed by chemometry: Towards development of the novel tool for clinical diagnosis. Anal Chim Acta. 2021;1177: 338784.

144. Liang X, Miao X, Xiao W, Ye Q, Wang S, Lin J, Li C, Huang Z. Filter-membrane-based ultrafiltration coupled with surface-enhanced Raman spectroscopy for potential differentiation of benign and malignant thyroid tumors from blood plasma. Int J Nanomed. 2020;15:2303–14.

145. Fang Y, Lin T, Zheng D, Zhu Y, Wang L, Fu Y, Wang H, Wu X, Zhang P. Rapid and label-free identification of different cancer types based on surface-enhanced Raman scattering profiles and multivariate statistical analysis. J Cell Biochem. 2021;122(2):277–89.

146. Haldavnekar R, Vijayakumar SC, Venkatakrishnan K, Tan B. Prediction of cancer stem cell fate by surface-enhanced Raman scattering functionalized nanoprobes. ACS Nano. 2020;14(11):15468–91.

147. Luo S, Ma L, Tian F, Gu Y, Li J, Zhang P, Yang G, Li H, Qu L-L. Fluorescence and surface-enhanced Raman scattering dual-mode nanoprobe for monitoring telomerase activity in living cells. Microchem J. 2022;175: 107171.

148. Kim HS, Lee T, Yun J, Lee G, Hong Y. Cancer protein biomarker identification and quantification using nanoforest substrate and hand-held Raman spectrometer. Microchem J. 2021;160: 105632.

149. Fang X, Zeng Q, Yan X, Zhao Z, Chen N, Deng Q, Zhu M, Zhang Y, Li S. Fast discrimination of tumor and blood cells by label-free surface-enhanced Raman scattering spectra and deep learning. J Appl Phys. 2021;129(12): 123103.

150. Fang X, Li S, Fu Q, Wang P, Wu X, Zhang Y. Label-free identification of lung cancer cells from blood cells based on surface-enhanced Raman scattering and support vector machine. Optik. 2021;248: 168157.

151. Culum NM, Cooper TT, Lajoie GA, Dayarathna T, Pasternak SH, Liu J, Fu Y, Postovit L-M, Lagugne-Labarthet F. Characterization of ovarian cancer-derived extracellular vesicles by surface-enhanced Raman spectroscopy. Analyst. 2021;146(23):7194–206.

152. Cheng NT, Chen DJ, Lou B, Fu J, Wang HY. A biosensing method for the direct serological detection of liver diseases by integrating a SERS-based sensor and a CNN classifier. Biosens Bioelectron. 2021;186: 113246.

153. Banaei N, Moshfegh J, Kim B. Surface enhanced Raman spectroscopy-based immunoassay detection of tumor-derived extracellular vesicles to differentiate pancreatic cancers from chronic pancreatitis. J Raman Spectrosc. 2021;52(11):1810–9.
154. Dawuti W, Zheng X, Liu H, Zhao H, Dou J, Sun L, Chu J, Lin R, Lue G. Urine surface-enhanced Raman spectroscopy combined with SVM algorithm for rapid diagnosis of liver cirrhosis and hepatocellular carcinoma. Photodiagnosis Photodyn Ther. 2022;38: 102811.
155. Liu K, Jin S, Song Z, Jiang L. High accuracy detection of malignant pleural effusion based on label-free surface-enhanced Raman spectroscopy and multivariate statistical analysis. Spectroc Acta Pt A-Molec Biomolec Spectr. 2020;226: 117632.
156. Roman M, Wrobel TP, Paluszkiewicz C, Kwiatek WM. Comparison between high definition FT-IR, Raman and AFM-IR for subcellular chemical imaging of cholesteryl esters in prostate cancer cells. J Biophotonics. 2020;13(5): e201960094.
157. Lombardini A, Mytskaniuk V, Sivankutty S, Andresen ER, Chen XQ, Wenger J, Fabert M, Joly N, Louradour F, Kudlinski A, Rigneault H. High-resolution multimodal flexible coherent Raman endoscope. Light Sci Appl. 2018;7:10.
158. Prince Richard C, Potma EO. Going visible:high-resolution coherent Raman imaging of cells and tissues. Light Sci Appl. 2019;8:10.
159. Lin H, Liao C-S, Wang P, Kong N, Cheng J-X. Spectroscopic stimulated Raman scattering imaging of highly dynamic specimens through matrix completion. Light Sci Appl. 2018;7:17179.
160. Chappard D, Guillaume B, Teman G, Kun-Darbois J-D. Raman spectroscopic analysis and imaging in two cases of benign cementoma: Comparison with dental and bone tissues. J Raman Spectrosc. 2020;51(7):1044–55.
161. Cordero E, Ruger J, Marti D, Mondol AS, Hasselager T, Mogensen K, Hermann GG, Popp J, Schie IW. Bladder tissue characterization using probe-based Raman spectroscopy: Evaluation of tissue heterogeneity and influence on the model prediction. J Biophotonics. 2020;13(2): e201960025.
162. Kujdowicz M, Placha W, Mech B, Chrabaszcz K, Okon K, Malek K. In vitro spectroscopy-based profiling of urothelial carcinoma: A Fourier transform infrared and Raman imaging study. Cancers. 2021;13(1):123.
163. Abramczyk H, Brozek-Pluska B, Kopec M, Surmacki J, Blaszczyk M, Radek M. Redox imbalance and biochemical changes in cancer by probing redox-sensitive mitochondrial cytochromes in label-free visible resonance Raman imaging. Cancers. 2021;13(5):960.
164. Straehle J, Erny D, Neidert N, Heiland DH, El Rahal A, Sacalean V, Steybe D, Schmelzeisen R, Vlachos A, Mizaikoff B, Reinacher PC, Coenen VA, Prinz M, Beck J, Schnell O. Neuropathological interpretation of stimulated Raman histology images of brain and spine tumors: part B. Neurosurg Rev. 2022;45(2):1721–9.
165. Neidert N, Straehle J, Erny D, Sacalean V, El Rahal A, Steybe D, Schmelzeisen R, Vlachos A, Reinacher PC, Coenen VA, Mizaikoff B, Heiland DH, Prinz M, Beck J, Schnell O. Stimulated Raman histology in the neurosurgical workflow of a major European neurosurgical center - part A. Neurosurg Rev. 2022;45(2):1731–9.
166. Marro M, Rodriguez-Rivero AM, Araujo-Andrade C, Fernandez-Figueras MT, Perez-Roca L, Castella E, Navines J, Mariscal A, Julian JF, Turon P, Loza-Alvarez P. Unravelling the encapsulation of DNA and other biomolecules in HAp microcalcifications of human breast cancer tissues by Raman imaging. Cancers. 2021;13(11):2658.
167. Liao Z, Lizio MG, Corden C, Khout H, Rakha E, Notingher I. Feasibility of integrated high-wavenumber Raman imaging and fingerprint Raman spectroscopy for fast margin assessment in breast cancer surgery. J Raman Spectrosc. 2020;51(10):1986–95.
168. Paidi SK, Shah V, Raj P, Glunde K, Pandey R, Barman I. Coarse Raman and optical diffraction tomographic imaging enable label-free phenotyping of isogenic breast cancer cells of varying metastatic potential. Biosens Bioelectron. 2021;175: 112863.
169. D'Acunto M, Gaeta R, Capanna R, Franchi A. Contribution of Raman spectroscopy to diagnosis and grading of chondrogenic tumors. Sci Rep. 2020;10(1):2155.
170. Brozek-Pluska B, Dziki A, Abramczyk H. Virtual spectral histopathology of colon cancer-biomedical applications of Raman spectroscopy and imaging. J Mol Liq. 2020;303: 112676.
171. Pekmezci M, Morshed RA, Chunduru P, Pandian B, Young J, Villanueva-Meyer JE, Tihan T, Sloan EA, Aghi MK, Molinaro AM, Berger MS, Hervey-Jumper SL. Detection of glioma infiltration at the tumor margin using quantitative stimulated Raman scattering histology. Sci Rep. 2021;11(1):12162.
172. Di L, Eichberg DG, Park YJ, Shah AH, Jamshidi AM, Luther EM, Lu VM, Komotar RJ, Ivan ME, Gultekin SH. Rapid Intraoperative diagnosis of meningiomas using stimulated Raman histology. World Neurosurg. 2021;150:E108–16.
173. Kar S, Jaswandkar SV, Katti KS, Kang JW, So PTC, Paulmurugan R, Liepmann D, Venkatesan R, Katti DR. Label-free discrimination of tumorigenesis stages using in vitro prostate cancer bone metastasis model by Raman imaging. Sci Rep. 2022;12(1):8050.
174. Roman M, Wrobel TP, Panek A, Paluszkiewicz C, Kwiatek WM. Lipid droplets in prostate cancer cells and effect of irradiation studied by Raman microspectroscopy. Biochim Biophys Acta Mol Cell Biol Lipids. 2020;1865(9): 158753.
175. Feng X, Fox MC, Reichenberg JS, Lopes FCPS, Sebastian KR, Dunn AK, Markey MK, Tunnell JW. Superpixel Raman spectroscopy for rapid skin cancer margin assessment. J Biophotonics. 2020;13(2): e201960109.
176. Fitzgerald CWR, Dogan S, Bou-Nassif R, McLean T, Woods R, Cracchiolo JR, Ganly I, Tabar V, Cohen MA. Stimulated Raman histology for rapid intra-operative diagnosis of sinonasal and skull base tumors. Laryngoscope. 2022;132(11):2142–7.
177. Shin KS, Francis AT, Hill AH, Laohajaratsang M, Cimino PJ, Latimer CS, Gonzalez-Cuyar LF, Sekhar LN, Juric-Sekhar G, Fu D. Intraoperative assessment of skull base tumors using stimulated Raman scattering microscopy. Sci Rep. 2019;9:20392.
178. Lee D, Du J, Yu R, Su Y, Heath JR, Wei L. Visualizing subcellular enrichment of glycogen in live cancer cells by stimulated Raman scattering. Anal Chem. 2020;92(19):13182–91.

179. Du J, Su Y, Qian C, Yuan D, Miao K, Lee D, Ng AHC, Wijker RS, Ribas A, Levine RD, Heath JR, Wei L. Raman-guided subcellular pharmaco-metabolomics for metastatic melanoma cells. Nat Commun. 2020;11(1):4830.

180. Boitor R, de Wolf C, Weesie F, Shipp DW, Varma S, Veitch D, Wernham A, Koloydenko A, Puppels G, Nijsten T, Williams HC, Caspers P, Notingher I. Clinical integration of fast Raman spectroscopy for Mohs micrographic surgery of basal cell carcinoma. Biomed Opt Express. 2021;12(4):2015–26.

181. Einstein EH, Ablyazova F, Rosenberg A, Harshan M, Wahl S, Har-El G, Constantino PD, Ellis JA, Boockvar JA, Langer DJ, D'Amico RS. Stimulated Raman histology facilitates accurate diagnosis in neurosurgical patients: A one-to-one noninferiority study. J Neuro-Oncol. 2022;159(2):369–75.

182. Giardina G, Micko A, Bovenkamp D, Krause A, Placzek F, Papp L, Krajnc D, Spielvogel CP, Winklehner M, Hoftberger R, Vila G, Andreana M, Leitgeb R, Drexler W, Wolfsberger S, Unterhuber A. Morpho-molecular metabolic analysis and classification of human pituitary gland and adenoma biopsies based on multimodal optical imaging. Cancers. 2021;13(13):3234.

183. Horgan CC, Nagelkerke A, Whittaker TE, Nele V, Massi L, Kauscher U, Penders J, Bergholt MS, Hood SR, Stevens MM. Molecular imaging of extracellular vesicles in vitro via Raman metabolic labelling. J Mat Chem B. 2020;8(20):4447–59.

184. Uematsu M, Kita Y, Shimizu T, Shindou H. Multiplex fatty acid imaging inside cells by Raman microscopy. Faseb J. 2020;34(8):10357–72.

185. Radwan B, Adamczyk A, Tott S, Czamara K, Kaminska K, Matuszyk E, Baranska M. Labeled vs. label-free Raman imaging of lipids in endothelial cells of various origins. Molecules. 2020;25(23):5752.

186. Abramczyk H, Imiela A, Surmacki J. Novel strategies of Raman imaging for monitoring intracellular retinoid metabolism in cancer cells. J Mol Liq. 2021;334: 116033.

187. Tipping WJ, Wilson LT, An C, Leventi AA, Wark AW, Wetherill C, Tomkinson NCO, Faulds K, Graham D. Stimulated Raman scattering microscopy with spectral phasor analysis: applications in assessing drug-cell interactions. Chem Sci. 2022;13(12):3468–76.

188. Bae K, Zheng W, Huang ZW. Spatial light-modulated stimulated Raman scattering (SLM-SRS) microscopy for rapid multiplexed vibrational imaging. Theranostics. 2020;10(1):312–22.

189. Sepp K, Lee M, Bluntzer MTJ, Helgason GV, Hulme AN, Brunton VG. Utilizing stimulated Raman scattering microscopy to study intracellular distribution of label-free ponatinib in live cells. J Med Chem. 2020;63(5):2028–34.

190. Lin P, Ni HL, Li HT, Vickers NA, Tan YY, Gong RY, Bifano T, Cheng JX. Volumetric chemical imaging in vivo by a remote-focusing stimulated Raman scattering microscope. Opt Express. 2020;28(20):30210–21.

191. Liu C, Xu T, Cheng G, Zhang X. Target-triggered regioselective assembly of nanoprobes for Raman imaging of dual cancer biomarkers in living cells. Sens Actuat B-Chem. 2021;330: 129319.

192. Chen H, Luo C, Zhang S. Intracellular imaging and concurrent pH sensing of cancer-derived exosomes using surface-enhanced Raman scattering. Anal Bioanal Chem. 2021;413(15):4091–101.

193. Gu Y, Bi X, Ye J. Gap-enhanced resonance Raman tags for live-cell imaging. J Mat Chem B. 2020;8(31):6944–55.

194. Yuan Y, Raj P, Zhang J, Siddhanta S, Barman I, Bulte JWM. Furin-mediated self-assembly of olsalazine nanoparticles for targeted Raman imaging of tumors. Angew Chem-Int Edit. 2021;60(8):3923–7.

195. de Albuquerque CDL, Schultz ZD. Super-resolution surface-enhanced Raman scattering imaging of single particles in cells. Anal Chem. 2020;92(13):9389–98.

196. Burgio F, Piffaretti D, Schmidt F, Pieles U, Reinert M, Ritz M-F, Saxer S. Tuning the surface chemistry of gold nanoparticles to specifically image glioblastoma cells using surface-enhanced Raman spectroscopy. ACS Appl Nano Mater. 2020;3(3):2447–54.

197. Bae K, Xin L, Zheng W, Tang C, Ang B-T, Huang Z. Mapping the intratumoral heterogeneity in glioblastomas with hyperspectral stimulated Raman scattering microscopy. Anal Chem. 2021;93(4):2377–84.

198. Yang Y, Yang Y, Liu Z, Guo L, Li S, Sun X, Shao Z, Ji M. Microcalcification-based tumor malignancy evaluation in fresh breast biopsies with hyperspectral stimulated Raman scattering. Anal Chem. 2021;93(15):6223–31.

199. Hollon TC, Orringer DA. An automated tissue-to-diagnosis pipeline using intraoperative stimulated Raman histology and deep learning. Mol Cell Oncol. 2020;7(3): e1736742.

200. Zhang Q, Yun KK, Wang H, Yoon SW, Lu F, Won D. Automatic cell counting from stimulated Raman imaging using deep learning. PLoS ONE. 2021;16(7): e0254586.

201. Liu Z, Su W, Ao J, Wang M, Jiang Q, He J, Gao H, Lei S, Nie J, Yan X, Guo X, Zhou P, Hu H, Ji M. Instant diagnosis of gastroscopic biopsy via deep-learned single-shot femtosecond stimulated Raman histology. Nat Commun. 2022;13(1):4050.

202. Hollon TC, Pandian B, Urias E, Save AV, Adapa AR, Srinivasan S, Jairath NK, Farooq Z, Marie T, Al-Holou WN, Eddy K, Heth JA, Khalsa SSS, Conway K, Sagher O, Bruce JN, Canoll P, Freudiger CW, Camelo-Piragua S, Lee H, Orringer DA. Rapid, label-free detection of diffuse glioma recurrence using intraoperative stimulated Raman histology and deep neural networks. Neuro Oncol. 2021;23(1):144–55.

203. Zhang LL, Wu YZ, Zheng B, Su LZ, Chen Y, Ma S, Hu QQ, Zou X, Yao L, Yang YL, Chen L, Mao Y, Chen Y, Ji MB. Rapid histology of laryngeal squamous cell carcinoma with deep-learning based stimulated Raman scattering microscopy. Theranostics. 2019;9(9):2541–54.

204. Suhito IR, Han Y, Ryu Y-S, Son H, Kim T-H. Autofluorescence-Raman mapping Integration analysis for ultra-fast label-free monitoring of adipogenic differentiation of stem cells. Biosens Bioelectron. 2021;178: 113018.

205. Xiong HQ, Qian NX, Miao YP, Zhao ZL, Chen C, Min W. Super-resolution vibrational microscopy by stimulated Raman excited fluorescence. Light Sci Appl. 2021;10:87.

206. Freudiger CW, Min W, Saar BG, Lu S, Holtom GR, He CW, Tsai JC, Kang JX, Xie XS. Label-free biomedical imaging with high sensitivity by stimulated Raman scattering microscopy. Science. 2008;322(5909):1857–61.

207. Ji MB, Orringer DA, Freudiger CW, Ramkissoon S, Liu XH, Lau D, Golby AJ, Norton I, Hayashi M, Agar NYR, Young GS, Spino C, Santagata S, Camelo-Piragua S, Ligon KL, Sagher O, Xie XS. Rapid, label-free detection of brain tumors with stimulated Raman scattering microscopy. Sci Transl Med. 2013;5(201):201ra119.

208. Orringer DA, Pandian B, Niknafs YS, Hollon TC, Boyle J, Lewis S, Garrard M, Hervey-Jumper SL, Garton HJL, Maher CO, Heth JA, Sagher O, Wilkinson DA, Snuderl M, Venneti S, Ramkissoon SH, McFadden KA, Fisher-Hubbard A, Lieberman AP, Johnson TD, Xie XS, Trautman JK, Freudiger CW, Camelo-Piragua S. Rapid intraoperative histology of unprocessed surgical specimens via fibre-laser-based stimulated Raman scattering microscopy. Nat Biomed Eng. 2017;1(2):0027.

209. Doherty T, McKeever S, Al-Attar N, Murphy T, Aura C, Rahman A, O'Neill A, Finn SP, Kay E, Gallagher WM, Watson RWG, Gowen A, Jackman P. Feature fusion of Raman chemical imaging and digital histopathology using machine learning for prostate cancer detection. Analyst. 2021;146(13):4195–211.

Publisher's Note

Springer Nature remains neutral with regard to jurisdictional claims in published maps and institutional affiliations.